

# $A_4$ realization of inverse seesaw: neutrino masses, $\theta_{13}$ and leptonic non-unitarity

Biswajit Karmakar<sup>a,1</sup>, Arunansu Sil<sup>a,2</sup>

<sup>a</sup> *Department of Physics, Indian Institute of Technology Guwahati, 781039 Assam, India*

## Abstract

We provide an  $A_4$  based flavor symmetric scenario to accommodate the inverse seesaw mechanism for explaining light neutrino masses and mixing. We find that the lepton mixing, in particular the tri-bimaximal mixing pattern and its deviation through nonzero  $\theta_{13}$ , is originated solely from the flavor structure of the lepton number violating contribution of the neutral lepton mass matrix. Here we discuss in detail how a nonzero value of  $\theta_{13}$  is correlated with the other parameters in the framework and its impact on the Dirac CP phase  $\delta$ . We also analyze the non-unitarity effects on lepton mixing matrix and its implication in terms of the lepton flavor violating decays, etc.

## 1 Introduction

Even after the discovery of the Higgs boson at LHC, understanding the origin of smallness associated with neutrino mass still remains an open question. In this respect seesaw mechanism serves as a guiding tool hinting toward the existence of new physics beyond the electroweak scale ( $v$ ). The conventional type-I seesaw [1–3] tries to explain the smallness of neutrino mass by adding three right-handed (RH) neutrinos  $N_{Ri=1,2,3}$  to the Standard Model (SM). They have Majorana mass  $M_R$  which is representative of the lepton number violation. With the Yukawa couplings of order unity, the left handed neutrinos can be light enough,  $m_\nu \sim v^2/M_R$ , provided the new physics scale  $M_R$  is sufficiently high  $\sim 10^{13}$  GeV or so. Though it suggests an interesting and natural explanation of why neutrinos are so light, such a high new physics scale is beyond the reach of present and future neutrino experiments.

Inverse seesaw [4, 5] on the other hand turns out to be a viable alternate scenario where the new physics scale responsible for neutrino mass generation can be brought down near TeV scale at the expense of involving additional fields (SM singlet fermions  $S_{i=1,2,3}$ ). In presence

---

<sup>1</sup>k.biswajit@iitg.ernet.in

<sup>2</sup>asil@iitg.ernet.in

of additional symmetry like a global  $U(1)_{B-L}$ , the corresponding neutral lepton  $9 \times 9$  mass matrix takes the form

$$M_\nu = \begin{pmatrix} 0 & m_D & 0 \\ m_D^T & 0 & M \\ 0 & M^T & 0 \end{pmatrix}, \quad (1.1)$$

using the basis  $(\nu_L^c, N_R, S)$ . Note that at this level, neutrinos are massless. Once the lepton number violating term  $\frac{1}{2}\overline{S^c}\mu S$  is introduced with  $\mu \ll m_D < M$ , the effective  $3 \times 3$  light neutrino mass matrix is given by

$$m_\nu = m_D M^{-1} \mu (M^T)^{-1} m_D^T = F \mu F^T, \quad (1.2)$$

where  $F = m_D M^{-1}$ . Since the lepton number turns out to be only an approximate symmetry of nature, it is perhaps more natural to be broken by a small amount  $\mu$  rather than by a large mass  $M_R$  as happened in case of type-I seesaw. Also note that the other mass scale  $M$  (say the new physics scale) in Eq. (1.1) can be as low as TeV since there exists a double suppression by this new physics scale through Eq.(1.2) and smallness of  $\mu$  is then justified to produce correct amount of light neutrino mass.

Apart from the smallness associated with the neutrino mass, the origin of lepton mixing matrix, being quite different from the quark mixing, needs to be understood. The study of underlying principle behind this typical mixing is particularly interesting with the recent finding of nonzero  $\theta_{13}$  [6–9]. The present global analysis [10–12] from several experimental data [13] can be summarized as

$$\begin{aligned} \Delta m_{21}^2 &= (7.11 - 8.18) \times 10^{-5} \text{ eV}^2, & |\Delta m_{31}^2| &= (2.30 - 2.65) \times 10^{-3} \text{ eV}^2, \\ \sin^2 \theta_{12} &= 0.278 - 0.375, & \sin^2 \theta_{23} &= 0.392 - 0.643, & \sin^2 \theta_{13} &= 0.0177 - 0.0294. \end{aligned}$$

In this regard, a particular pattern yielding  $\tan^2 \theta_{23} = 1$ ,  $\tan^2 \theta_{12} = 1/2$  and  $\theta_{13} = 0$  is called the tri-bimaximal mixing (TBM) [14]. It has received a lot of attention as such a pattern can be elegantly generated using flavor symmetries. Use of non-Abelian discrete symmetries (for a review see [15]) like  $A_4, S_4$  etc. is very well known [16, 17] in this context. However a deformation from TBM mixing becomes essential after the precise measurement of  $\theta_{13}$ . The details of such deformation are studied for type-I [18, 19] and type-II seesaw [20] in the context of  $A_4$ . In general, extra flavon fields (SM singlet scalar fields transforming non-trivially under the flavor symmetry) are employed<sup>3</sup>. for this approach [21, 22]. Once these fields get their vacuum expectation values (vev), the requisite flavor structure is generated.

---

<sup>3</sup> Deviations from TBM mixing can also be realized by perturbing the vev alignments of the  $A_4$  scalars involved [18].

In this work we aim to study the lepton mixing matrix in the inverse seesaw framework based on an  $A_4$  flavor symmetry. In its minimal form, ref [23] discusses how a TBM pattern can be incorporated in an  $A_4$  symmetric inverse seesaw scenario. They have shown (among one of the few possibilities discussed there) that if  $m_D, M$  and  $\mu$  matrices all possess the following structure:

$$M_0 = \begin{pmatrix} X & 0 & 0 \\ 0 & Y & Z \\ 0 & Z & Y \end{pmatrix}, \quad (1.3)$$

the light neutrino mass matrix obtains a typical form, [24]

$$m_\nu = \begin{pmatrix} A & B & B \\ B & A + D & B - D \\ B & B - D & A + D \end{pmatrix}. \quad (1.4)$$

The diagonalizing matrix of the above form of  $m_\nu$  is representative of the TBM mixing in the basis where charged lepton mass matrix is diagonal. In [25], authors have shown that in a  $S_4$  based inverse seesaw, nonzero  $\theta_{13}$  can be generated from the correction in the charged lepton sector. Few earlier attempts in realizing inverse seesaw in the framework of discrete flavor symmetries can be found in [26]. Here the construction is such that the charged lepton mass matrix becomes diagonal. Now with a simpler form for  $m_D$  and  $M$  (where  $X = Z$  and  $Y = 0$  in  $M_0$ ),  $F$  in Eq. (1.2) becomes proportional to identity matrix and hence the structure of  $\mu$  matrix coincides with that of  $m_\nu$ . This means that  $\mu$  matrix (and hence  $m_\nu$  matrix also) of the form similar to  $M_0$  would generate the TBM pattern of lepton mixing matrix. Therefore we finally adopt a  $\mu$  matrix different from  $M_0$  structure so as to accommodate the observed value of  $\theta_{13}$ . It is interesting to note that in the inverse seesaw,  $\mu$  matrix (the coefficient matrix of the  $\overline{S^c}S$  term) being different from zero is the source of violation of the lepton number as stated earlier and now it also turns out that the same  $\mu$  is also the source of non-zero  $\theta_{13}$  as well as other mixings (the charged lepton mass matrix is diagonal) in our scenario. This is a salient feature of our model. We have then discussed the possible correlation between the Dirac CP phase ( $\delta$ ) with  $\theta_{13}$  and other parameters involved. We have tried to address the smallness associated with the  $\mu$  term by considering its origin from a higher dimensional operator. The  $A_4$  symmetry along with other non-Abelian discrete symmetries like  $Z_4 \times Z_3$  play important role. We have estimated the effective neutrino mass parameter associated with neutrinoless double beta decay [27, 28] and studied the correlation with  $\delta$  as well.

Furthermore  $m_D$  being close to  $M$ , in general the inverse seesaw framework allows non-negligible mixing between the light and heavy neutrino states resulting non-unitarity contributions to the lepton flavor mixing. Since the flavor structure is completely known in our

framework, we are then able to study the non-unitarity involved in the set-up and in turn constrain some of the parameters. Lepton flavor violating (LFV) decays also result from this non-unitarity effect. However it turns out in our scenario that branching ratio of those LFV decays are vanishingly small due to exact cancellation of elements involved followed from the particular flavor structure we have considered.

This paper is organized as follows. In the Section 2 below, we describe the construction of the model based on the symmetries of the framework. The detailed phenomenology constraining the parameters of the model from the available data of neutrino experiments takes place in Section 3 and 4. Section 5 is devoted in studying the non-unitarity effect and we comment on lepton flavor violating decays and additional contribution to neutrinoless double beta decay. Finally we conclude in Section 6.

## 2 The Model

In order to realize the usual inverse seesaw mechanism for the generation of light neutrino masses, we extend the SM particle content by introducing three RH neutrinos,  $N_{Ri=1,2,3}$ , and three other singlet fermions,  $S_{i=1,2,3}$  as already mentioned. In addition few flavons ( $\phi_S, \phi_T, \xi, \xi', \rho$ ) are included to understand the flavor structure of the lepton mixing. An additional global  $U(1)_{B-L}$  symmetry is considered along with the flavor symmetry  $A_4 \times Z_4 \times Z_3$ . The field content of the model and their charges under the symmetry of the model (appropriate for the discussion) are mentioned in Table 1. Once the flavon fields get vev (along suitable directions), the desired structures of the mass matrices are generated as we will find below.

Fields	$e_R$	$\mu_R$	$\tau_R$	$L$	$H$	$N_R$	$S$	$\phi_S$	$\phi_T$	$\xi$	$\xi'$	$\rho$
$A_4$	1	$1'$	$1''$	3	1	3	3	3	3	1	$1'$	1
$Z_4$	$-i$	$-i$	$-i$	$-i$	1	$-i$	1	-1	1	-1	-1	$i$
$Z_3$	1	1	1	1	1	1	$\omega^2$	1	1	1	1	$\omega$
$B-L$	-1	-1	-1	-1	0	-1	1	-2	0	-2	-2	0

Table 1: Fields content and transformation properties under the symmetries imposed on the model.

The charged lepton Yukawa terms in the Lagrangian are given by<sup>4</sup>,

$$\mathcal{L}_l = \frac{y_e}{\Lambda} (\bar{L}\phi_T) H e_R + \frac{y_\mu}{\Lambda} (\bar{L}\phi_T)' H \mu_R + \frac{y_\tau}{\Lambda} (\bar{L}\phi_T)'' H \tau_R, \quad (2.1)$$

to the leading order, where  $\Lambda$  represents the cut-off scale of the theory and  $y_e, y_\mu$  and  $y_\tau$  are the respective coupling constants. Terms within the first parenthesis describe the product

---

<sup>4</sup> In Eq. (2.1), one can introduce a contribution like  $\bar{L}\phi_T^\dagger H e_R$ . But such a term can be absorbed in the original contribution by a mere redefinition of the coupling.

of two  $A_4$  triplets, which further contracts with  $A_4$  singlets  $1$ ,  $1''$  and  $1'$  corresponding to  $e_R, \mu_R$  and  $\tau_R$  fields respectively to constitute a true  $A_4$  singlet.  $A_4$  multiplication rules can be summarized as:  $1' \times 1' = 1''$ ,  $1' \times 1'' = 1$ ,  $1'' \times 1'' = 1'$  and  $3 \times 3 = 1 + 1' + 1'' + 3_A + 3_S$ . Further details about  $A_4$  group can be found in [24]. Now we choose the vev of  $\phi_T$  as  $\langle \phi_T \rangle = v_T(1, 0, 0)$  [17] so that the charged lepton mass matrix turns out to be diagonal in the leading order and can be written as  $M_l = v \frac{v_T}{\Lambda} \text{diag}(y_e, y_\mu, y_\tau)$ .

The allowed terms in the neutrino sector invariant under the symmetries considered are given by:

$$\mathcal{L}_\nu = y_1 \bar{L} \tilde{H} N_R + y_2 \overline{N_R^c} S \rho + (\mu_1 \xi \rho^2 / \Lambda^2 + \mu_2 \phi_S \rho^2 / \Lambda^2) \overline{S^c} S + \mu_3 \overline{S^c} S \xi' \rho^2 / \Lambda^2, \quad (2.2)$$

where  $y_i, \mu_i$  are the respective couplings. To construct the flavor structures we consider the flavons acquire vevs along  $\langle \phi_S \rangle = v_S(1, 1, 1)$ ,  $\langle \xi \rangle = v_\xi$ ,  $\langle \xi' \rangle = v_{\xi'}$  and  $\langle \rho \rangle = v_\rho$ . In appendix A, we have written the complete scalar potential invariant under  $A_4 \times Z_4 \times Z_3$  and the additional global  $U(1)_{B-L}$  symmetry. There we have argued that such choices of vev alignments are indeed possible. With such vev alignment Eq. (2.2) yields the following  $9 \times 9$  mass matrix  $M_\nu$  in the basis  $(\nu_L^c, N_R, S)$

$$M_\nu = \begin{pmatrix} 0 & m_D & 0 \\ m_D^T & 0 & M \\ 0 & M^T & \mu \end{pmatrix}. \quad (2.3)$$

The  $3 \times 3$  mass matrices present in Eq. (2.3) are

$$m_D = y_1 v \begin{pmatrix} 1 & 0 & 0 \\ 0 & 0 & 1 \\ 0 & 1 & 0 \end{pmatrix}; M = y_2 v_\rho \begin{pmatrix} 1 & 0 & 0 \\ 0 & 0 & 1 \\ 0 & 1 & 0 \end{pmatrix} \quad \text{and} \quad (2.4)$$

$$\mu = \begin{pmatrix} a - 2b/3 & b/3 & b/3 \\ b/3 & -2b/3 & a + b/3 \\ b/3 & a + b/3 & -2b/3 \end{pmatrix} + \begin{pmatrix} 0 & 0 & d \\ 0 & d & 0 \\ d & 0 & 0 \end{pmatrix}, \quad (2.5)$$

with  $a = 2\mu_1 v_\xi v_\rho^2 / \Lambda^2$ ,  $b = -2\mu_2 v_S v_\rho^2 / \Lambda^2$  and  $d = 2\mu_3 v_\xi' v_\rho^2 / \Lambda^2$ . Note that  $\mu$  term follows from a higher dimensional contribution and hence is expected to be naturally small compared to  $m_D$  and  $M$ .

### 3 Neutrino masses and Mixings

The specific flavor structure of the model ensures that (as evident from Eq. (1.2) and Eq. (2.4))  $F = m_D M^{-1} \propto \mathbb{I}$ . Hence in our set-up, the effective light neutrino mass matrix

becomes

$$m_\nu = F\mu F^T = \frac{v^2 y_1^2}{v_\rho^2 y_2^2} \mu. \quad (3.1)$$

Eq. (3.1) clearly shows that the flavor structure of  $m_\nu$  matrix is entirely dictated by that of  $\mu$ . Such an interesting feature was also pointed out in [29], calling it screening mechanism in the context of double seesaw. Additionally we note here that  $\mu$  serves the purpose of generating non-zero  $\theta_{13}$  as well with a modification of its original TBM structure (similar to  $M_0$  in Eq. (1.3)). This makes our model an interesting scenario to study, as the source of  $\theta_{13}$  is connected with the lepton number violating parameter ( $\mu$ ). Now let us focus our attention to the  $\mu$  matrix in Eq. (2.5). It is well known from the very specific structure of the first matrix of right hand side of Eq. (2.5) involving  $a, b$  only [17] that it leads to a TBM pattern of the lepton mixing matrix (as the charged lepton mass matrix is diagonal), given by

$$U_{TB} = \begin{pmatrix} \sqrt{\frac{2}{3}} & \frac{1}{\sqrt{3}} & 0 \\ -\frac{1}{\sqrt{6}} & \frac{1}{\sqrt{3}} & -\frac{1}{\sqrt{2}} \\ -\frac{1}{\sqrt{6}} & \frac{1}{\sqrt{3}} & \frac{1}{\sqrt{2}} \end{pmatrix}, \quad (3.2)$$

resulting  $\theta_{13} = 0$ . The second matrix in Eq. (2.5) breaks the TBM pattern and we expect a deviation of  $\theta_{13}$  from zero. To find out the deviation and possible correlations between the mixing angles and parameters of the model, we first rotate  $m_\nu$  from Eq. (3.1) by  $U_{TB}$  so as to get

$$m'_\nu = U_{TB}^T m_\nu U_{TB}, \quad (3.3)$$

$$= \frac{v^2 y_1^2}{v_\rho^2 y_2^2} \begin{pmatrix} a - b - d/2 & 0 & \sqrt{3}d/2 \\ 0 & a + d & 0 \\ \sqrt{3}d/2 & 0 & -a - b + d/2 \end{pmatrix}. \quad (3.4)$$

As evident, a further rotation by  $U_1$  (another unitary matrix) in the 13 plane will diagonalize the light neutrino mass matrix, *i.e.*  $m_\nu^{diag} = U_1^T m'_\nu U_1$ . The angle  $\theta$  and phase  $\psi$  associated in  $U_1$  are therefore related with the parameters  $a, b, d$  involved in  $m_\nu$ <sup>5</sup>.

Let us consider the form of  $U_1$  as,

$$U_1 = \begin{pmatrix} \cos \theta & 0 & \sin \theta e^{-i\psi} \\ 0 & 1 & 0 \\ -\sin \theta e^{i\psi} & 0 & \cos \theta \end{pmatrix}, \quad (3.5)$$

---

<sup>5</sup>The overall factor  $\frac{y_1^2 v^2}{y_2^2 v_\rho^2}$  does not take part in determining the mixing angles and phases. However it would be important in determining the exact magnitude of light neutrino masses as we will see later.

where  $\theta$  and  $\psi$  are the angle and phase respectively. The diagonalization of  $m_\nu$  takes place through

$$(U_{TB}U_1)^T m_\nu U_{TB}U_1 = \text{diag}(m_1 e^{i\gamma_1}, m_2 e^{i\gamma_2}, m_3 e^{i\gamma_3}), \quad (3.6)$$

where  $m_{i=1,2,3}$  are the real and positive eigenvalues and  $\gamma_{i=1,2,3}$  are the phases extracted from the corresponding complex eigenvalues. We are now in a position to evaluate the effective light neutrino mixing  $U_\nu$  such that  $U_\nu^T m_\nu U_\nu = \text{diag}(m_1, m_2, m_3)$ . The  $U_\nu$  then becomes  $U_\nu = U_{TB}U_1U_m$ , where  $U_m = \text{diag}(1, e^{i\alpha_{21}/2}, e^{i\alpha_{31}/2})$  is the Majorana phase matrix with  $\alpha_{21} = (\gamma_1 - \gamma_2)$  and  $\alpha_{31} = (\gamma_1 - \gamma_3)$ , one common phase being irrelevant. Now this  $U_\nu$  (charged lepton mass matrix being diagonal) can be compared with  $U_{PMNS}$  which in its standard parametrization is given by [30],

$$U_{PMNS} = \begin{pmatrix} c_{12}c_{13} & s_{12}c_{13} & s_{13}e^{-i\delta} \\ -s_{12}c_{23} - c_{12}s_{13}s_{23}e^{i\delta} & c_{12}c_{23} - s_{12}s_{13}s_{23}e^{i\delta} & c_{13}s_{23} \\ s_{12}s_{23} - c_{12}s_{13}c_{23}e^{i\delta} & -c_{12}s_{23} - s_{12}s_{13}c_{23}e^{i\delta} & c_{13}c_{23} \end{pmatrix} U_m, \quad (3.7)$$

where  $c_{ij} = \cos \theta_{ij}$ ,  $s_{ij} = \sin \theta_{ij}$ , the angles  $\theta_{ij} = [0, \pi/2]$ ,  $\delta = [0, 2\pi]$  is the CP-violating Dirac phase while  $\alpha_{21}$  and  $\alpha_{31}$  are the two CP-violating Majorana phases.

We consider  $a = |a|e^{i\phi_a}$ ,  $b = |b|e^{i\phi_b}$  and  $d = |d|e^{i\phi_d}$  (*i.e.* they are in general complex) the phases of which are indicated by  $\phi_{a,b,d}$ . For calculational purpose, we define parameters  $|\alpha| = |b|/|a|$ ,  $|\beta| = |d|/|a|$  and the difference of phases by  $\phi_{ba} = \phi_b - \phi_a$  and  $\phi_{da} = \phi_d - \phi_a$ . As  $U_1$  diagonalizes the  $m'_\nu$  matrix in Eq. (3.3),  $\theta$  and  $\psi$  can be expressed in terms of  $a, b$  and  $d$  as,

$$\tan 2\theta = \frac{\sqrt{3}\beta \cos \phi_{da}}{(\beta \cos \phi_{da} - 2) \cos \psi + 2\alpha \sin \phi_{ba} \sin \psi}, \quad (3.8)$$

$$\tan \psi = \frac{\sin \phi_{da}}{\alpha \cos(\phi_{ba} - \phi_{da})}. \quad (3.9)$$

Comparing  $U_\nu = U_{TB}U_1U_m$  with  $U_{PMNS}$  as in Eq.(3.7), we obtain the following expressions for  $\theta_{13}$  and Dirac CP phase  $\delta$  [20]

$$\sin \theta_{13} = \sqrt{\frac{2}{3}} |\sin \theta|, \quad \delta = \arg[(U_1)_{13}]. \quad (3.10)$$

These correlations are among the usual characteristics of the  $A_4$  flavor symmetry [22, 31–33]. For  $\sin \theta > 0$  (depending on the choices of  $\alpha, \beta$ ), the relation  $\delta = \arg[(U_1)_{13}]$  implies  $\delta = \psi$ . Again if  $\sin \theta < 0$ , the relation becomes  $\delta = \psi \pm \pi$ . Hence for both the cases, we have  $\tan \psi = \tan \delta$  and Eq. (3.9) becomes

$$\tan \delta = \frac{\sin \phi_{da}}{\alpha \cos(\phi_{ba} - \phi_{da})}. \quad (3.11)$$

Using Eq. (3.6), the complex light neutrino mass eigenvalues are evaluated as

$$m_{1,3}^c = \frac{v^2 y_1^2}{v_\rho^2 y_2^2} \left[ -b \pm \sqrt{a^2 - ad + d^2} \right], \quad (3.12)$$

$$m_2^c = \frac{v^2 y_1^2}{v_\rho^2 y_2^2} (a + d). \quad (3.13)$$

The real and positive mass eigenvalues ( $m_i$ ) can be then extracted having the following expressions,

$$m_1 = k \left[ (P - \alpha \cos \phi_{ba})^2 + (Q - \alpha \sin \phi_{ba})^2 \right]^{1/2}, \quad (3.14)$$

$$m_2 = k \left[ 1 + \beta^2 + 2\beta \cos \phi_{da} \right]^{1/2}, \quad (3.15)$$

$$m_3 = k \left[ (P + \alpha \cos \phi_{ba})^2 + (Q + \alpha \sin \phi_{ba})^2 \right]^{1/2}, \quad (3.16)$$

where  $k = |a|v^2|y_1|^2/v_\rho^2|y_2|^2$  and

$$P = \left[ \frac{1}{2}(A + \sqrt{A^2 + B^2}) \right]^{1/2}, \quad Q = \left[ \frac{1}{2}(-A + \sqrt{A^2 + B^2}) \right]^{1/2}, \quad (3.17)$$

$$A = 1 + \beta^2 \cos 2\phi_{da} - \beta \cos \phi_{da}, \quad B = \beta^2 \sin 2\phi_{da} - \beta \sin \phi_{da}. \quad (3.18)$$

The three phases associated with these mass eigenvalues are  $\gamma_i = \phi_i + \phi_0$ , where  $\phi_0$  is the overall phase for  $ay_1^2/y_2^2$  and  $\phi_i$  are given by

$$\begin{aligned} \phi_1 &= \tan^{-1} \left( \frac{Q - \alpha \sin \phi_{ba}}{P - \alpha \cos \phi_{ba}} \right), \\ \phi_2 &= \tan^{-1} \left( \frac{\beta \sin \phi_{da}}{1 + \beta \cos \phi_{da}} \right), \\ \phi_3 &= \tan^{-1} \left( \frac{Q + \alpha \sin \phi_{ba}}{P + \alpha \cos \phi_{ba}} \right). \end{aligned} \quad (3.19)$$

Note that the Majorana phases  $\alpha_{21}$  and  $\alpha_{31}$  depend on  $\phi_i$  only.

## 4 Constraining parameters from neutrino data

Using Eqs.(3.14-3.16) one can define a ratio of solar to the atmospheric mass-squared differences as

$$r = \frac{\Delta m_\odot^2}{|\Delta m_{atm}^2|}, \quad (4.1)$$

with  $\Delta m_\odot^2 \equiv \Delta m_{21}^2 = m_2^2 - m_1^2$  and  $|\Delta m_{atm}^2| \equiv |\Delta m_{31}^2| = |m_3^2 - m_1^2|$ . From the expressions above in Section 3, it is clear that neutrino mixing angle  $\theta_{13}$ , Dirac CP phase  $\delta$ , Majorana phases ( $\alpha_{21} = \phi_1 - \phi_2$  and  $\alpha_{31} = \phi_1 - \phi_3$ ) and ratio  $r$  are functions of four parameters,  $\alpha, \beta, \phi_{ba}$  and  $\phi_{da}$ . The other two angles ( $\theta_{23}, \theta_{12}$ ) are obtained from the comparison between



$U_\nu$  and  $U_{PMNS}$ . Among these,  $\theta_{13}, \theta_{23}, \theta_{12}$  and ratio  $r$  are precisely known from the neutrino oscillation data. Since  $\delta$  (also the Majorana phases) is yet not be known from the experimental data, we perform the analysis for several choices of  $\delta$ . Then the four parameters can be constrained using values of  $\theta_{13}, r$  and  $\delta$  once we keep one of them fixed. For convenience, we have divided our analysis into five cases: (i) Case A [ $\phi_{ba} = \phi_{da} = 0$ ], (ii) Case B [ $\phi_{ba} = 0$ ], (iii) Case C [ $\phi_{da} = 0$ ], (iv) Case D [ $\phi_{ba} = \phi_{da} = \phi$ ] and (v) the General Case.

Following [10], the best fit values of  $\Delta m_{\odot}^2 = 7.6 \times 10^{-5} \text{ eV}^2$  and  $|\Delta m_{atm}^2| = 2.48 \times 10^{-3} \text{ eV}^2$  along with their  $3\sigma$  ranges are used for our analysis. We have fixed  $r$  at 0.03. Though there exists another parameter  $k$  (see Eqs. (3.14-3.16)), this cancels out in the expression for  $r$ . The magnitude of  $k$  will be fixed in order to reproduce the solar or atmospheric mass square difference(s). Once this is also obtained, we essentially get the estimate of the absolute neutrino masses and Majorana phases. Expression for the effective neutrino mass parameter  $|m_{ee}|$  appearing in the neutrinoless double beta decay is given by [30],

$$|m_{ee}| = \left| m_1 c_{12}^2 c_{13}^2 + m_2 s_{12}^2 c_{13}^2 e^{i\alpha_{21}} + m_3 s_{13}^2 e^{i(\alpha_{31} - 2\delta)} \right|. \quad (4.2)$$

Hence we have a prediction for  $|m_{ee}|$  for the allowed range of parameters. Note that in this analysis we should be able to find out values of  $\alpha, \beta, k, \phi_{ba}, \phi_{da}$  and  $\delta$  which are consistent with experimental data. However the scales involved as flavons vev, cut-off scale  $\Lambda$ , order of  $\mu$  matrix (*i.e.* the magnitude of  $|a|, |b|, |d|$ ) can not be determined, specifically here in this section. Latter while discussing the non-unitarity effects in Section 5, we would be able to set limits on those scales.

#### 4.1 Case A: [ $\phi_{ba} = \phi_{da} = 0$ ]

In this case, we make the simplest choice for the associated phases as  $\phi_{ba} = \phi_{da} = 0$ . Then Eq. (3.8 and 3.10) can be written as

$$\tan 2\theta = \frac{\sqrt{3}\beta}{(\beta - 2)} \quad \text{and} \quad \sin \theta_{13} = \sqrt{\frac{2}{3}} |\sin \theta|, \quad (4.3)$$

with  $\tan \delta = 0$ . Hence we note that  $\sin \theta_{13}$  solely depends on  $\beta$ . With  $\beta = 0$  we get back the TBM pattern of neutrino mixing matrix. In Fig. 1 left panel, we plot the variation of  $\sin \theta_{13}$  against  $\beta$  using Eq. (4.3) the  $3\sigma$  range of  $\sin \theta_{13}$  (between 0.133 and 0.177 as indicated by the two horizontal lines) predicts a range of  $\beta$ : = 0.328 – 0.413 (denoted by the vertical lines).

With  $\phi_{ba} = \phi_{da} = 0$ , expressions of absolute neutrino masses in Eq. (3.14-3.16) simplify into,

$$m_1 = k \left| \sqrt{1 + \beta^2 - \beta} - \alpha \right|, \quad (4.4)$$

$$m_2 = k [1 + \beta], \quad (4.5)$$

$$m_3 = k \left[ \sqrt{1 + \beta^2 - \beta} + \alpha \right]. \quad (4.6)$$

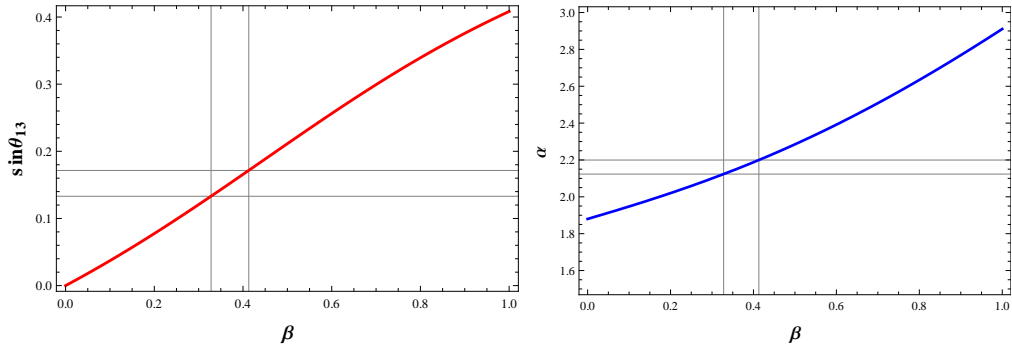


Figure 1: [Left panel] Plot for  $\sin \theta_{13}$  vs  $\beta$ . Here  $3\sigma$  range for  $\sin \theta_{13}$  fixes  $\beta$  in the range 0.328-0.413. [Right panel]  $r = 0.03$  contour in the  $\alpha$ - $\beta$  plane.

Thereby the ratio of solar to atmospheric mass-squared differences,  $r$  (as defined in Eq. (4.1)), now takes the form

$$r = \frac{1}{2} - \frac{\alpha^2 - 3\beta}{4\alpha\sqrt{1 + \beta^2 - \beta}}. \quad (4.7)$$

Note that this ratio depends upon both  $\alpha$  and  $\beta$ . To understand this dependence in a better way, we draw the contour plot for  $r = 0.03$  [30] in  $\alpha - \beta$  plane as shown in Fig. 1 (right panel). We find that the allowed range of  $\beta$  from Fig. 1 (left panel) indicates a range of the other parameter  $\alpha$  to be within (2.12 - 2.18) as seen from Fig. 1 (right panel). Note that contour plot of  $r$  provides a one to one correspondence between  $\alpha$  and  $\beta$  values within this range. For example, the best fit values of  $\sin \theta_{13}$  and  $r$  corresponds to  $\alpha = 2.16$  and  $\beta = 0.372$ . So the sets of  $(\alpha, \beta)$  values within this allowed range would be used for rest of our analysis in Case A. It is observed that  $\theta_{12}$  and  $\theta_{23}$  also fall within their  $3\sigma$  value [10] for the entire allowed range of  $\alpha$  and  $\beta$ .

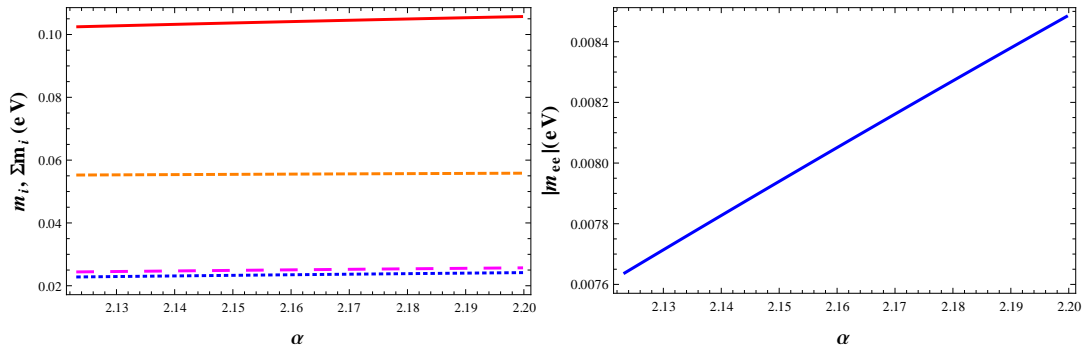


Figure 2: [Left panel] Absolute neutrino masses vs  $\alpha$  (blue dotted, magenta large dashed, orange dashed and red continuous lines represent  $m_1$ ,  $m_2$ ,  $m_3$  and  $\sum m_i$  respectively); [Right panel] Plot for  $|m_{ee}|$  vs  $\alpha$  [Case A].

Parameters/Observables	Allowed Range
$\beta$	0.328-0.412
$\alpha$	2.12-2.18
$k$ (eV)	$1.84 \times 10^{-2} - 1.82 \times 10^{-2}$
$\sum m_i$ (eV)	0.102462 - 0.105713
$ m_{ee} $ (eV)	0.0076-0.0085

Table 2: Range of  $\beta, \alpha, k, \sum m_i$  and  $|m_{ee}|$  for  $3\sigma$  variation of  $\sin \theta_{13}$  [Case A].

From Eq. (4.4-4.6) it is evident that along with  $\alpha$  and  $\beta$ , individual absolute light neutrino masses depend also upon another parameter  $k(= |a|v^2|y_1|^2/v_\rho^2|y_2|^2)$ . Once we know the sets of  $(\alpha, \beta)$  that produces  $\sin \theta_{13}$  in the  $3\sigma$  allowed range and  $r = 0.03$ , it is possible to determine  $k$  from the best fit values of solar (or atmospheric) mass square differences,  $m_2^2 - m_1^2 = 7.6 \times 10^{-5} \text{ eV}^2$  ( $|\Delta m_{atm}^2| = 2.48 \times 10^{-3} \text{ eV}^2$ ) [10]. Hence corresponding to a set  $(\alpha, \beta)$ , we can determine  $k$ . Doing so, we find the allowed range for  $k$  turns out to be  $(1.82 - 1.84) \times 10^{-2} \text{ eV}$ . Using such a set of values of  $(\alpha, \beta, k)$  we plot the sum of the light neutrino masses and effective mass parameter  $|m_{ee}|$  for neutrinoless double beta decay in the left and right panels of Fig. 2 respectively. Our findings are summarized in Table 2 in terms of allowed ranges for parameters and observables.

#### 4.2 Case B: [ $\phi_{ba} = 0$ ]

With  $\phi_{ba} = 0$ , Eqs. (3.8) and (3.9) reduce into

$$\tan 2\theta = \frac{\sqrt{3}\beta \cos \phi_{da}}{(\beta \cos \phi_{da} - 2) \cos \psi}, \quad \tan \delta = \frac{\tan \phi_{da}}{\alpha}. \quad (4.8)$$

As before,  $\sin \theta_{13}$  can be obtained from the relation  $\sin \theta_{13} = \sqrt{\frac{2}{3}} |\sin \theta|$ . Using Eqs.(3.14-3.16), the ratio of solar to atmospheric mass squared differences in this case can be written as

$$r = \frac{1}{4\alpha P} [1 + \beta^2 + 2\beta \cos \phi_{da} - (P - \alpha)^2 - Q^2], \quad (4.9)$$

where  $P$  and  $Q$  are same as given in Eqs. (3.18).

The above expressions show that  $\sin \theta_{13}$  and  $r$  both are dependent on three parameters namely  $\alpha, \beta$  and  $\phi_{da}$  contrary to Case A where they depend only on two parameters  $\alpha$  and  $\beta$ . However if we choose a particular  $\delta$ , we can replace  $\phi_{da}$  dependence in terms of  $\alpha$  by using the second relation from Eq.(4.8). Then if we draw contours of  $r$  and  $\sin \theta_{13}$  in the  $\alpha, \beta$  plane where a simultaneous satisfaction of best fit values of  $\sin \theta_{13}$  and  $r$  provide solutions for  $\alpha$  and  $\beta$  with that specific choice of  $\delta$ . As an example, we have drawn contour plots for

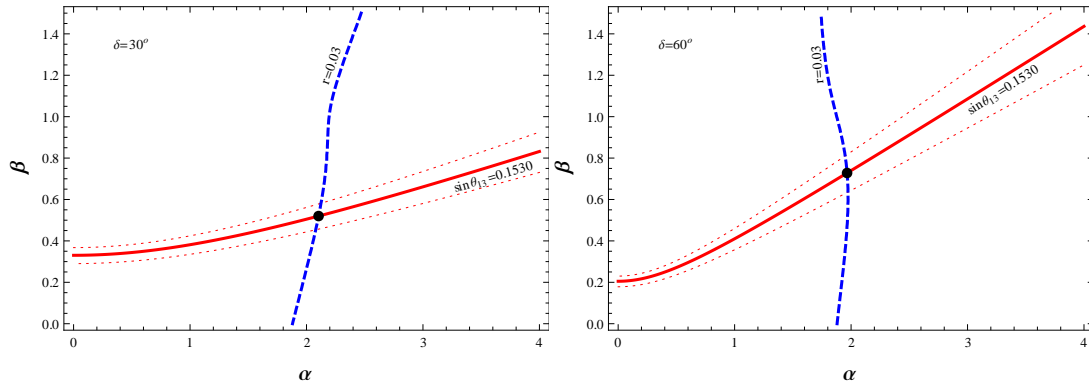


Figure 3: Contour plot for  $r = 0.03$  (dashed line) and  $\sin \theta_{13} = 0.153$  (continuous line) for  $\delta = 30^\circ$  (left panel) and  $\delta = 60^\circ$  (right panel) respectively. Red dotted lines represent a  $3\sigma$  variation of  $\sin \theta_{13}$  while black dots stand for intersection (solution) points for best fit values of  $\sin \theta_{13}$  and  $r$  in both panels.

$\delta$	$\alpha$	$\beta$	$k$ (eV)	$\Sigma m_i$ (eV)	$ m_{ee} $ (eV)
$0^\circ$	2.162	0.372	0.0183	0.1042	0.0222
$10^\circ$	2.155	0.393	0.0184	0.1047	0.0225
$20^\circ$	2.136	0.448	0.0188	0.1065	0.0233
$30^\circ$	2.103	0.521	0.0195	0.1093	0.0245
$40^\circ$	2.060	0.596	0.0204	0.1128	0.0260
$50^\circ$	2.011	0.666	0.0213	0.1162	0.0274
$60^\circ$	1.965	0.728	0.0220	0.1182	0.0280
$70^\circ$	1.928	0.782	0.0221	0.1179	0.0275
$80^\circ$	1.901	0.827	0.0217	0.1152	0.0259
$90^\circ$	1.879	0.859	0.0210	0.1109	0.0270

Table 3: Parameters satisfying neutrino oscillation data for various values of  $\delta$  with  $\phi_{ba} = 0$  [Case B].

$\sin \theta_{13} = 0.153$  and  $r = 0.03$  in Fig. 3 for  $\delta = 30^\circ$  (left panel) and  $\delta = 60^\circ$  (right panel) in  $\alpha - \beta$  plane. Intersecting points between the  $\sin \theta_{13}$  and  $r$  contours in these plots, denoted by black dots represent the set of solutions  $(\alpha, \beta)$  satisfying neutrino oscillation data.  $\theta_{12}$  and  $\theta_{23}$  fall in the right range for the entire  $3\sigma$  range of  $\sin \theta_{13}$  considered. With each such set of solution points  $(\alpha, \beta)$  for a fixed  $\delta$ , we can compute the other parameter  $k$  in order to obtain the correct solar (or atmospheric) mass splitting. Here in Table 3 we have provided sets of values for  $(\alpha, \beta, k)$  for various  $\delta$  satisfying  $\sin \theta_{13} = 0.153$  and  $r = 0.03$  obtained from neutrino oscillation experiments.

It is to be noted that with a particular choice of  $\delta$ , contour plots for both  $\sin \theta_{13}$  and  $r$  are

identical with the one obtained from  $|\pi - \delta|$ . Here in this set-up, scanning over all values of  $\delta$  (with  $3\sigma$  variation of  $\sin\theta_{13}$  taken into account), sum of the three light neutrino masses and effective mass parameter are predicted to be in the range :  $0.104 \text{ eV} \lesssim \Sigma m_i \lesssim 0.118 \text{ eV}$  and  $0.022 \text{ eV} \lesssim |m_{ee}| \lesssim 0.028 \text{ eV}$ . These are mentioned in the two rightmost columns in Table 3.

### 4.3 Case C: [ $\phi_{da} = 0$ ]

We consider here the other possibility of choosing one of the two phases as zero, *i.e.*  $\phi_{da} = 0$ . Then we have relations  $\tan 2\theta = \frac{\sqrt{3}\beta}{(\beta-2)}$ ,  $\sin\theta_{13} = \sqrt{\frac{2}{3}}|\sin\theta|$  with  $\tan\delta = 0$ . This coincides with Eq. (4.3) of Case A. Hence we can use the outcome of Fig. 1 (left panel) for specifying the range of  $\alpha, \beta$  which reproduce the value of  $\sin\theta_{13}$  (with in  $3\sigma$  allowed range) and  $r$  respectively. With  $\phi_{da} = 0$ , the real and positive mass eigenvalues take the form

$$m_1 = k \left[ (\sqrt{1 + \beta^2 - \beta} - \alpha \cos \phi_{ba})^2 + (\alpha \sin \phi_{ba})^2 \right]^{1/2}, \quad (4.10)$$

$$m_2 = k [1 + \beta], \quad (4.11)$$

$$m_3 = k \left[ (\sqrt{1 + \beta^2 - \beta} + \alpha \cos \phi_{ba})^2 + (\alpha \sin \phi_{ba})^2 \right]^{1/2}. \quad (4.12)$$

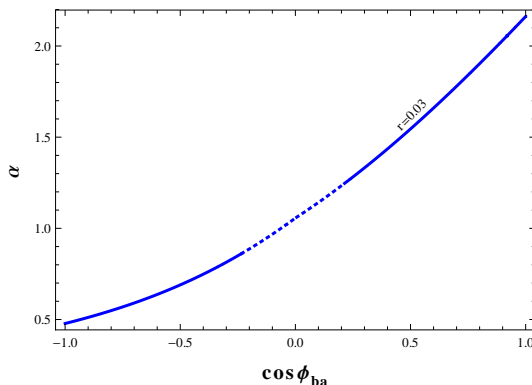


Figure 4: Contour plot for  $r = 0.03$  in the  $\alpha - \cos \phi_{ba}$  plane for  $\phi_{ba} = 0$ . The disallowed range of  $\alpha, \cos \phi_{ba}$  is indicated by the dotted portion.

In this case, the ratio of solar to atmospheric mass-squared differences  $r$ , is related to the parameters by the relation,

$$r = \frac{3\beta - \alpha^2 + 2\alpha \cos \phi_{ba} \sqrt{1 + \beta^2 - \beta}}{4\alpha \sqrt{1 + \beta^2 - \beta} |\cos \phi_{ba}|}. \quad (4.13)$$

The Eq. (4.13) describes a relation between parameters  $\alpha, \beta$  and  $\phi_{ba}$ . We fix  $\beta$  at 0.372 which corresponds to the best fit value of  $\sin\theta_{13} = 0.153$  as seen from Fig. 1 (left panel). Then  $\cos \phi_{ba}$  and  $\alpha$  correlation is addressed through a contour plot of  $r = 0.03$  in Fig. 4 using

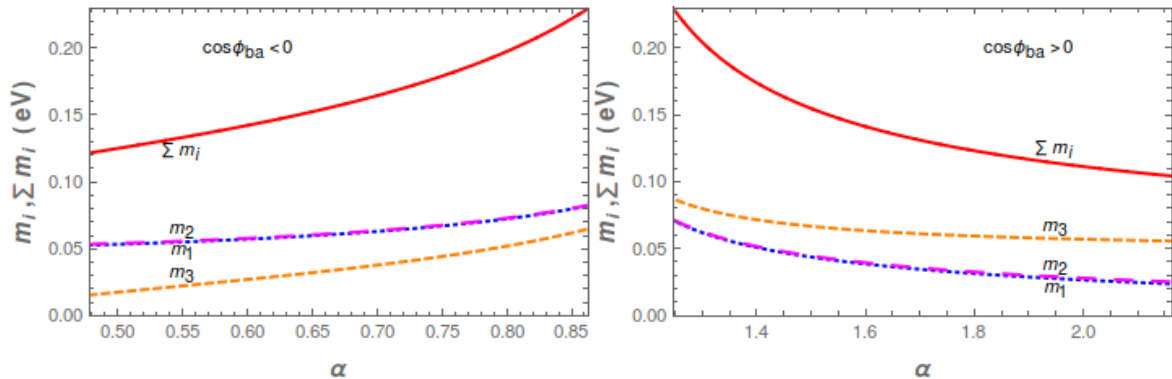


Figure 5: Absolute neutrino masses vs  $\alpha$  (blue dotted, magenta large dashed, orange dashed and red continuous lines represent  $m_1$ ,  $m_2$ ,  $m_3$  and  $\sum m_i$  respectively). The left panel is for  $\cos \phi_{ba} < 0$  and right panel is for  $\cos \phi_{ba} > 0$ .

Eq. (4.13). We find for  $-1 \leq \cos \phi_{ba} \leq 1$ ,  $\alpha$  falls with the region  $0.478 \leq \alpha \leq 2.162$ . This range is further constrained once we use cosmological constraint on sum of the light neutrino masses to be below 0.23 eV [34]. This exclusion part is indicated by the dotted portion of the  $r$  contour in Fig. 4. Now in order to have an estimate of absolute neutrino masses, first we need to know the other parameter  $k$ . Corresponding to the fixed value of  $\beta = 0.372$ , we have sets of values of  $(\cos \phi_{ba}, \alpha)$  which leads to  $r = 0.03$  from Fig.4. For each such set of  $(\cos \phi_{ba}, \alpha)$ , we can have the corresponding  $k$  value in order to get the best fit value for solar mass squared difference,  $m_2^2 - m_1^2 = 7.6 \times 10^{-5} \text{ eV}^2$ , and obtain

$$k = \left[ \frac{7.6 \times 10^{-5}}{4\alpha r \sqrt{1 + \beta^2 - \beta} |\cos \phi_{ba}|} \right]^{1/2}, \quad (4.14)$$

where the Eqs. (4.10, 4.13) are employed and  $\beta = 0.372$  is taken. In Fig. 5 (left panel and right panel) we have plotted absolute neutrino masses ( $m_i$ ) against  $\alpha$  (with  $\beta = 0.372$ ) where one to one correspondence between  $\alpha$  and  $\cos \phi_{ba}$  ( $< 0$  and  $> 0$ ) from Fig. 4 is taken into account. Here  $m_1, m_2, m_3$  and  $\sum m_i$  are denoted by blue dotted, magenta large dashed orange dashed and red continuous lines respectively. Note that  $\cos \phi_{ba} < 0$  indicates the inverted hierarchy while  $\cos \phi_{ba} > 0$  corresponds to the normal hierarchy for light neutrinos. We have found the prediction for  $|m_{ee}|$  to be within  $0.016 \text{ eV} < |m_{ee}| < 0.052 \text{ eV}$  for normal hierarchy and  $0.047 \text{ eV} < |m_{ee}| < 0.066 \text{ eV}$  for inverted hierarchy considering the restricted variation of  $\alpha$  ( $0.478 \leq \alpha \leq 0.863$  for  $\cos \phi_{ba} < 0$  and  $1.247 \leq \alpha \leq 2.162$  for  $\cos \phi_{ba} > 0$ ). Few of our findings are tabulated in Table 4.

$\alpha$	$\cos \phi_{ba}$	$k$	$\sum m_i$	$ m_{ee} $
1.904	0.8	0.0218 eV	0.1164 eV	0.0194 eV
0.814	-0.3	0.0544 eV	0.0231 eV	0.0604 eV

Table 4: Representative values of  $k$ ,  $\sum m_i$  and  $|m_{ee}|$  in Case C.

#### 4.4 Case D: [ $\phi_{ba} = \phi_{da} = \phi_a$ ]

Now, if we consider  $\phi_{ba} = \phi_{da} = \phi$ , then Eqs. 3.8 and 3.9 can be written as

$$\tan 2\theta = \frac{\sqrt{3}\beta \cos \phi}{(\beta \cos \phi - 2) \cos \psi + 2\alpha \sin \phi \sin \psi}, \quad \tan \delta = \tan \psi = \frac{\sin \phi}{\alpha}. \quad (4.15)$$

and hence  $\sin \theta_{13}$  again can be computed using the relation  $\sin \theta_{13} = \sqrt{\frac{2}{3}} |\sin \theta|$ . The real and positive mass eigenvalues now take the form

$$\begin{aligned} m_1 &= k [(P_D - \alpha \cos \phi)^2 + (Q_D - \alpha \sin \phi)^2]^{1/2}, \\ m_2 &= k [1 + \beta^2 + 2\beta \cos \phi]^{1/2}, \\ m_3 &= k [(P_D + \alpha \cos \phi)^2 + (Q_D + \alpha \sin \phi)^2]^{1/2}, \end{aligned}$$

with

$$P_D = \left[ \frac{1}{2} \left( A_D + \sqrt{A_D^2 + B_D^2} \right) \right]^{1/2}, \quad Q_D = \left[ \frac{1}{2} \left( -A_D + \sqrt{A_D^2 + B_D^2} \right) \right]^{1/2}, \quad (4.16)$$

$$A_D = 1 + \beta^2 \cos 2\phi - \beta \cos \phi, \quad B_D = \beta^2 \sin 2\phi - \beta \sin \phi. \quad (4.17)$$

Using above expressions for light neutrino masses we can write the ratio of solar to atmospheric mass squared difference as

$$r = \frac{(1 + \beta^2 + 2\beta \cos \phi) - (P_D - \alpha \cos \phi)^2 - (Q_D - \alpha \sin \phi)^2}{4\alpha(P_D \cos \phi + Q_D \sin \phi)}. \quad (4.18)$$

Clearly just like Case B, here also both  $\sin \theta_{13}$  and  $r$  both depends on  $\alpha, \beta$  and the common phase  $\phi$ . Following the same prescription as in Case B, one can draw contours for best fit values of  $\sin \theta_{13}$  and  $r$  in the  $\alpha, \beta$  plane. Intersecting points of these two contours then represent simultaneous solutions for both  $\alpha$  and  $\beta$  for a particular value of  $\delta$ . In Fig. 6 we have drawn such contours for  $\delta = 30^\circ$  (left panel) and  $\delta = 60^\circ$  (right panel) for demonstrative purpose. In this plot, black dots represent the intersecting points for  $\sin \theta_{13} = 0.153$  and  $r = 0.03$  contours and hence the solutions for  $\alpha$  and  $\beta$ . Here we find that solutions satisfying neutrino oscillation data exist for all values of  $\delta$  between  $0^\circ$  and  $90^\circ$  as given in Table 5. We find that the contour plots for both  $\sin \theta_{13} = 0.1530$  and  $r = 0.03$  with a specific  $\delta$  value coincides (and hence the solutions for  $\alpha, \beta$ ) with the one with other  $\delta$  values (in the range  $0$  to  $2\pi$ ) obtained from  $|\pi - \delta|$ .

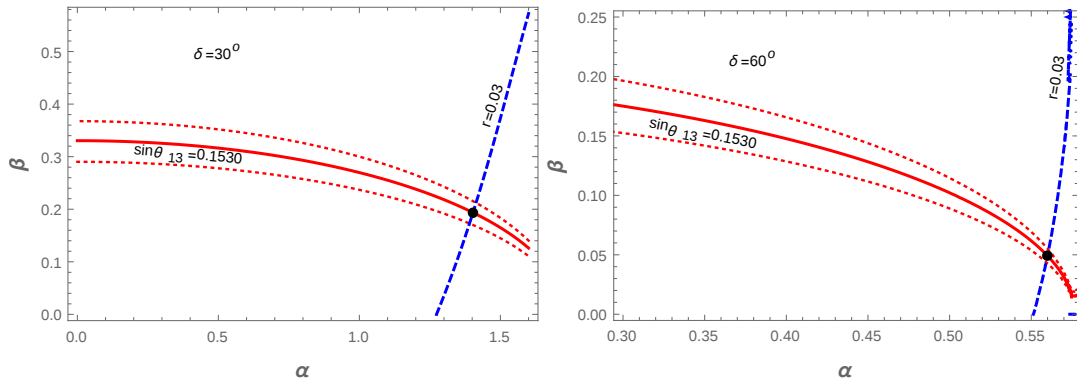


Figure 6: Contour plot for  $r = 0.03$  (dashed line) and  $\sin \theta_{13} = 0.153$  (continuous line) for  $\delta = 30^\circ$  (left panel) and  $\delta = 60^\circ$  (right panel) respectively. Red dotted lines represent a  $3\sigma$  variation  $\sin \theta_{13}$  and black dots stands for solution points for best fit values of  $\sin \theta_{13}$  and  $r$  in both panels.

$\delta$	$\alpha$	$\beta$	$k$ (eV)	$\Sigma m_i$ (eV)	$ m_{ee} $ (eV)
$0^\circ$	2.162	0.372	0.0183	0.1042	0.0220
$10^\circ$	2.039	0.343	0.0194	0.1057	0.0221
$20^\circ$	1.755	0.272	0.0223	0.1095	0.0214
$30^\circ$	1.403	0.194	0.0273	0.1187	0.0225
$40^\circ$	1.070	0.131	0.0354	0.1365	0.0319
$50^\circ$	0.792	0.084	0.0472	0.1659	0.0447
$60^\circ$	0.560	0.049	0.0658	0.2159	0.0641
$62^\circ$	0.518	0.043	0.0701	0.2301	0.0694
$70^\circ$	0.359	0.023	0.1011	0.3157	0.1000
$80^\circ$	0.175	0.006	0.2027	0.6144	0.2022

Table 5: Parameters satisfying neutrino oscillation data for various values of  $\delta$  with  $\phi_{ba} = \phi_{ba} = \phi$  [Case D].

Following the same algorithm as described in Case B, in the last two column of Table 5 we have listed allowed values for sum of all three light neutrinos and effective mass parameter. Therefore varying  $\delta$  between 0 to  $2\pi$ , we find range of few quantities as  $0.1042 \text{ eV} \lesssim \Sigma m_i \lesssim 0.6144 \text{ eV}$  and  $0.0220 \text{ eV} \lesssim |m_{ee}| \lesssim 0.2022 \text{ eV}$  respectively. Therefore imposing the constraint  $\Sigma m_i < 0.23 \text{ eV}$  on sum of all three light neutrinos coming from Planck [34], the allowed range for  $\delta$  gets restricted and it finally lies in the range  $0^\circ \leq \delta < 62^\circ$  (in terms of the full range  $0^\circ - 360^\circ$ , other allowed ranges are  $128^\circ - 180^\circ$  and  $180^\circ - 242^\circ$ ,  $308^\circ - 360^\circ$ ). In this case only the normal hierarchy results as in Case A and B.



## 4.5 General Case

In the previous sub-sections, we have considered four different cases with specific choices for  $\phi_{ba}$  and/or  $\phi_{da}$  for our analysis on neutrino masses and mixing. Here we discuss the most general case where we allow the variation of  $\phi_{ba}$  and  $\phi_{da}$  for their entire range between 0 and  $2\pi$ . For this purpose, we employ Eqs. (3.8-3.10) in order to analyze the mixing angles. On the other hand, the ratio of solar to the atmospheric mass-squared differences  $r$ , defined in Eq. (4.1), can also be computed once we use the general expressions for absolute neutrino masses given in Eq. (3.14-3.16).

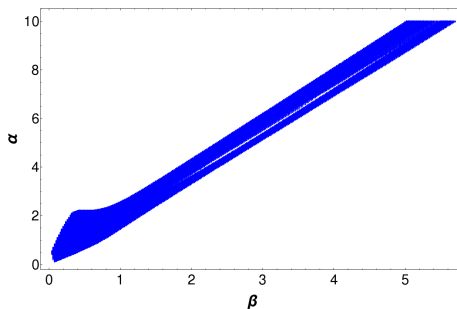


Figure 7: Allowed range (represented by the blue patch) of  $\alpha$  and  $\beta$  in order to satisfy  $3\sigma$  range of  $\sin\theta_{13}$  and  $r$ . The phases  $\phi_{ba,da}$  are allowed to vary within 0 to  $2\pi$ .

Now using the  $3\sigma$  allowed ranges for  $\theta_{13}$  and  $r$  [10], we represent the allowed regions for  $\alpha$  and  $\beta$  in Fig. 7 represented by the blue patch. Here  $\phi_{ba}$  and  $\phi_{da}$  are allowed to vary within their full range (0 to  $2\pi$ ). However it turns out that only a portion of this entire range can actually satisfy the required  $\theta_{13}$  and  $r$  through Eqs. (3.8-3.10) along with the range of  $\alpha - \beta$  depicted in Fig. 7. This is shown in Fig. 8 in the  $\phi_{ba} - \phi_{da}$  plane. Knowing the allowed range

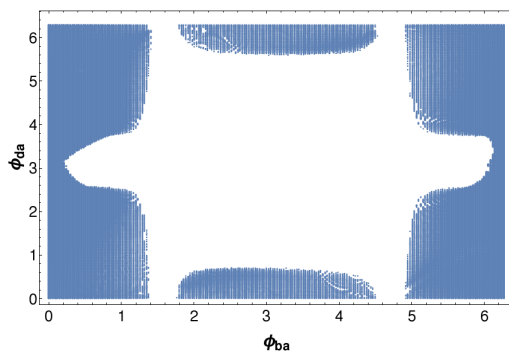


Figure 8: Allowed ranges of  $\phi_{ba}$  and  $\phi_{da}$  in order to produce  $\sin\theta_{13}$  in the  $3\sigma$  range, correct  $r$ , satisfying  $\sum m_i < 0.23$  eV.

of  $\alpha$ ,  $\beta$  and their correlation with phases  $\phi_{ba}$ ,  $\phi_{da}$ , we plot in Fig. 9 the prediction of the model in terms of sum of the three light neutrino masses ( $\sum m_i$ ) in the left panel and effective

mass parameter for neutrinoless double beta decay ( $|m_{ee}|$ ) in the right panel as functions of  $\beta$ . In the left panel of Fig. 9, the horizontal orange patch represents the excluded region by the upper bound on sum of the absolute neutrino masses  $\sum m_i \leq 0.23$  eV, whereas in the right panel of the same figure we have already included this additional constraint to plot  $|m_{ee}|$ . Finally in Fig. 10, we show the allowed range of the Dirac CP phase  $\delta$  against the range of

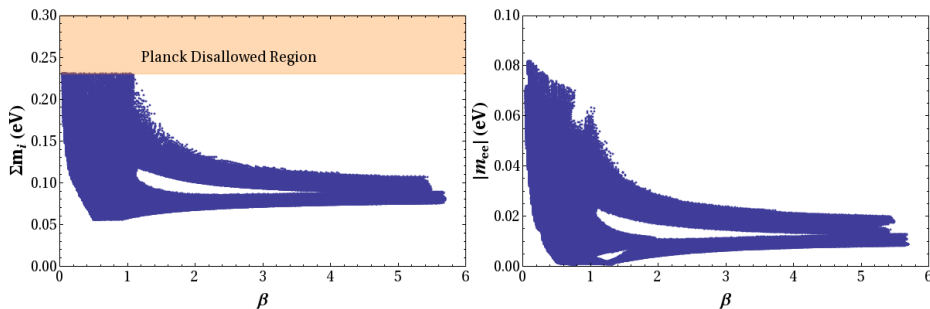


Figure 9: [Left panel]  $\sum m_i$  vs  $\beta$  which satisfy  $3\sigma$  range of  $\sin \theta_{13}$  and  $r$ . Horizontal orange patch represents the excluded region from the upper bound on sum of all the three light neutrino masses ( $\sum m_i < 0.23$  eV). [Right panel]  $|m_{ee}|$  vs  $\beta$  satisfying  $\sum m_i < 0.23$  eV. In both the panels  $\alpha, \phi_{ba}$  and  $\phi_{da}$  vary according to Figs. 7-8.

$\beta$  (allowed) where we consider simultaneously the corresponding allowed range of  $\alpha, \phi_{ba}$  and  $\phi_{da}$  following Figs. 7-9.

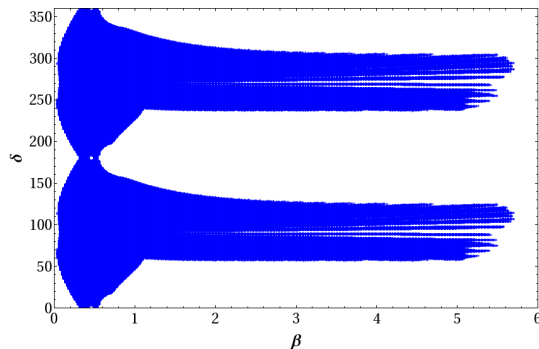


Figure 10: Dirac CP phase  $\delta$  vs  $\beta$  satisfying constraints from  $3\sigma$  range of  $\sin \theta_{13}$  and  $r$  (with  $\sum m_i < 0.23$  eV). Here both  $\phi_{ba}$  and  $\phi_{da}$  varies between  $0 - 2\pi$ .

## 5 Non-unitary effect

In Section 3, we have determined the neutrino mixing matrix  $U_\nu$  and identify it with the  $U_{PMNS}$  (charged lepton mass matrix being diagonal) as it diagonalizes the effective light neutrino mass matrix  $m_\nu$  through the unitary transformation  $U_\nu^T m_\nu U_\nu = \text{diag}(m_1, m_2, m_3)$ .

However the  $U_{PMNS}$  should receive a correction over  $U_\nu$  as the heavy states carries an admixture with the light neutrinos [35]. To clarify, suppose  $V_\nu$  is the diagonalizing matrix which makes  $M_\nu$  into the block diagonal form first, *i.e.*

$$V_\nu^T M_\nu V_\nu = \begin{pmatrix} m_{\nu_{light} 3 \times 3} & 0_{3 \times 6} \\ 0_{6 \times 3} & m_{\nu_{heavy} 6 \times 6} \end{pmatrix}. \quad (5.1)$$

At this point the light neutrino mass matrix  $m_{\nu_{light}} \simeq -m_\nu = -m_D M^{-1} \mu (M^T)^{-1} m_D^T$  and the other one is given by

$$m_{\nu_{heavy}} \simeq \begin{pmatrix} 0 & M^T \\ M & \mu \end{pmatrix}, \quad (5.2)$$

in the lowest order [36]. Let  $U$  be the matrix of the form

$$U = \begin{pmatrix} U_\nu & 0 \\ 0 & U_h \end{pmatrix}, \quad (5.3)$$

which will do the individual diagonalization, *i.e.*  $U_\nu$  and  $U_h$  are expected to diagonalize  $m_{\nu_{light}}$  and  $m_{\nu_{heavy}}$  respectively (remember that  $U_\nu$  is the diagonalizing matrix of  $m_\nu$  as already discussed in Section 3). So finally  $W = V_\nu U$  diagonalizes the entire  $9 \times 9$  matrix  $M_\nu$  such that  $W^T M_\nu W = \text{diag}(m_{i=1,2,3}, m_{N_{k=1,2,\dots,6}})$ . One can decompose  $W$  as follows:

$$W = \begin{pmatrix} W_{3 \times 3} & W_{3 \times 6} \\ W_{6 \times 3} & W_{6 \times 6} \end{pmatrix}, \quad (5.4)$$

where the block  $W_{3 \times 3}$  is the leading order replacement of  $U_{PMNS}$  matrix which is non-unitary [37, 38]. It is shown [37, 40] that  $W_{3 \times 3} \simeq (\mathbb{I} - \frac{1}{2} F F^\dagger) U_\nu$ , where the non unitary effect is parametrized by

$$\eta = \frac{1}{2} F F^\dagger, \quad (5.5)$$

with  $F = m_D M^{-1}$  as defined before. The present bound on  $\eta$  (at 90% C.L.) can be summarized as [39]

$$|\eta| < \begin{pmatrix} 2.0 \times 10^{-3} & 3.5 \times 10^{-5} & 8.0 \times 10^{-3} \\ 3.5 \times 10^{-5} & 8.0 \times 10^{-4} & 5.1 \times 10^{-3} \\ 8.0 \times 10^{-3} & 5.1 \times 10^{-3} & 2.7 \times 10^{-3} \end{pmatrix}. \quad (5.6)$$

In our case  $F$  is proportional to identity as mentioned before and so as  $\eta$ . In the present framework  $\eta$  turns out to satisfy  $|\eta| = \frac{v^2 |y_1|^2}{2v_\rho^2 |y_2|^2} \mathbb{I} = C_1 \mathbb{I}$  say, and hence the above bound on  $\eta$  can be translated into

$$C_1 < 8.0 \times 10^{-4}, \quad (5.7)$$

where  $C_1 = v^2|y_1|^2/2v_\rho^2|y_2|^2$ . Using this bound, we can now estimate the scales involved in our scenario, *i.e.*  $v_\rho, \Lambda$  etc. For simplicity we assume all the flavons have the same vevs  $v_f$ . Then  $C_1$  is given by  $\lambda v^2/2v_f^2$  where  $\lambda = |y_1|^2/|y_2|^2$ . Hence the common flavon vev  $v_f$  is bounded by

$$v_f > 6.15\sqrt{\lambda} \text{ TeV}, \quad (5.8)$$

which follows from Eq.(5.7).

## 5.1 Determining the scales ( $v_f, \Lambda$ ) involved in the set-up

Note that the parameter  $k$  defined in Section 3 can be written as

$$k = \frac{\lambda v^2}{v_f^2} |a| = 2\lambda |\mu_1| \frac{v_f v^2}{\Lambda^2}, \quad (5.9)$$

once the common flavon vev  $v_f$  is assumed and  $a = 2\mu_1 v_f^3/\Lambda^2$  is inserted. As we already have an estimate for the range of  $k$  for all cases (A, B, C and D), we can use that input on  $k$  to study the correlation between  $v_f$  and  $\Lambda$  for various choices of  $\lambda$  while  $|\mu_1|$  is fixed, say at unity. This correction however satisfy Eq. (5.8) and we discuss it below case by case.

### 5.1.1 Case A: [ $\phi_{ba} = \phi_{da} = 0$ ]

In this case, we have found  $k = 0.0183$  eV corresponding to the set of parameters  $\alpha, \beta$  ( $\alpha = 2.16, \beta = 0.372$ ) which produces the best fit value of  $\sin \theta_{13} = 0.1530$  and  $r = 0.03$  so as to have the solar and atmospheric mass squared splittings  $7.6 \times 10^{-5} \text{ eV}^2$  and  $2.48 \times 10^{-3} \text{ eV}^2$  respectively via Eqs. (4.4-4.6). Now using this particular value of  $k$ , we employ Eq.(5.9)

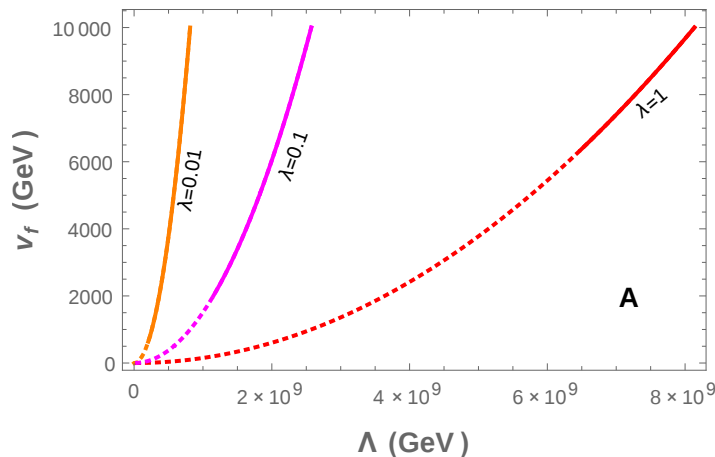


Figure 11: Contour plots for  $k = 0.0183$  eV in the  $v_f - \Lambda$  plane (using Eq. (5.9)) for  $\phi_{ba} = \phi_{da} = 0$  (and  $|\mu_1| = 1$ ). The dotted portion in each curve indicates the excluded part in view of Eq. (5.8). Here the orange, magenta and red line stands for  $\lambda = 0.01, 0.1$  and  $1$  respectively.

	$\lambda = 0.01$	$\lambda = 0.1$	$\lambda = 1$
$\Lambda$ in GeV (for $C_1 = 7.5 \times 10^{-4}$ )	$2.06 \times 10^8$	$1.16 \times 10^9$	$6.48 \times 10^9$
$\Lambda$ in GeV (for $C_1 = 4 \times 10^{-4}$ )	$2.40 \times 10^8$	$1.35 \times 10^9$	$7.59 \times 10^9$

Table 6: Cutoff scale  $\Lambda$  for different  $C_1$  (with  $\phi_{da} = \phi_{ba} = 0$ ) when  $\lambda = 0.01, 0.1$  and  $1$ .

to have an estimate of  $v_f$  and  $\Lambda$  once the couplings  $\lambda$  and  $|\mu_1|$  are fixed. In Fig. 11, we plot the contour lines for  $k = 0.0183$  eV in the  $v_f - \Lambda$  plane for different choices of  $\lambda$ . Here  $|\mu_1|$  is assumed to be unity for simplicity. Following Eq. (5.8), the  $v_f - \Lambda$  correlation gets further constrained. Depending on the specific choices of  $\lambda$ , the lower bound on  $v_f$  is obtained through Eq. (5.8). The portion of each  $k$  contour line which does not satisfy Eq.(5.8) is indicated by the dotted segment. Note that corresponding to a specific choice of the non-unitarity parameter  $\eta$ ,  $v_f$  would be fixed through  $C_1 = \frac{\lambda v^2}{2v_f^2}$  (for fixed  $\lambda$ ) which then indicates a particular  $\Lambda$ . In Table 6, we provide some such specific choices of  $\Lambda$  corresponding to different choices of  $\eta$ . We find that with  $\lambda$  small enough, the cut-off scale can also be lowered  $\sim$  TeV.

### 5.1.2 Case B: [ $\phi_{ba} = 0$ ]

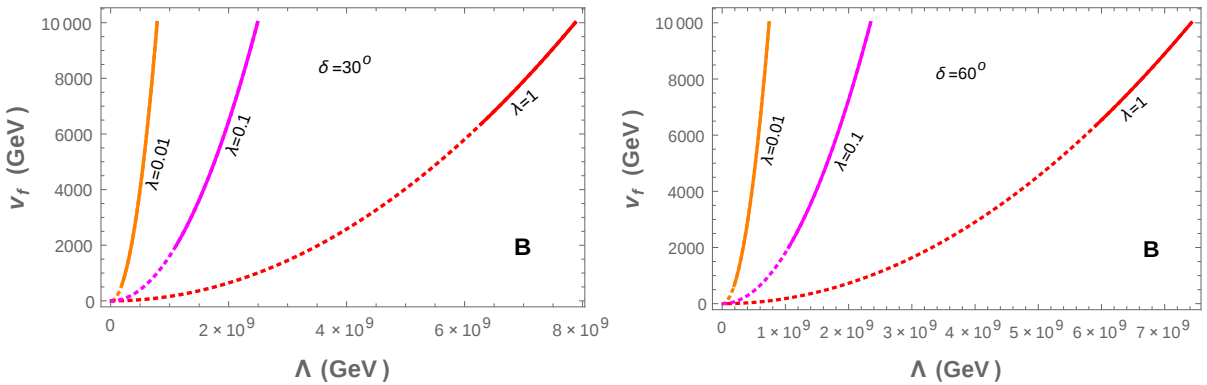


Figure 12: [Left panel] Contour plot for  $k = 0.0195$  eV in the  $v_f - \Lambda$  plane for  $\phi_{ba} = 0$  and  $\delta = 30^\circ$ . [Right panel] Contour plot for  $k = 0.0220$  eV in the  $v_f - \Lambda$  plane for  $\phi_{ba} = 0$  and  $\delta = 60^\circ$ . In both the panels orange, magenta and red lines stand for  $\lambda = 0.01, 0.1$  and  $1$  respectively.

	$C_1 = 7.5 \times 10^{-4}$			$C_1 = 4 \times 10^{-4}$		
	$\lambda = 0.01$	$\lambda = 0.1$	$\lambda = 1$	$\lambda = 0.01$	$\lambda = 0.1$	$\lambda = 1$
$\Lambda$ in GeV ( $\delta = 30^\circ$ )	$1.98 \times 10^8$	$1.12 \times 10^9$	$6.3 \times 10^9$	$2.32 \times 10^8$	$1.31 \times 10^9$	$7.34 \times 10^9$
$\Lambda$ in GeV ( $\delta = 60^\circ$ )	$1.89 \times 10^8$	$1.05 \times 10^9$	$5.9 \times 10^9$	$2.19 \times 10^8$	$1.23 \times 10^9$	$6.92 \times 10^9$

Table 7: Cutoff scale  $\Lambda$  for different  $C_1$  (with  $\phi_{ba} = 0$ ) and  $\lambda$  ( $= 0.01, 0.1$  and  $1$ ).

In Section 4 we have seen that for  $\phi_{ba} = 0$ ,  $r$  and  $\sin\theta_{13}$  depend not only on  $\alpha, \beta$ , but also on the choice of Dirac CP phase  $\delta$ . We have already listed our finding toward this dependency in Table 3. Corresponding to each  $\delta$ , we have sets of  $(\alpha, \beta)$  and  $k$  from Table 3. Now for a fixed  $\delta$  and  $k$  we can study the correlation of  $v_f$  and  $\Lambda$  in a similar way as described in Case A above. In Fig. 12, we have studied this correlation for two different choices for  $\delta = 30^\circ$ ,  $k = 0.0195$  eV (left panel) and  $\delta = 60^\circ$ ,  $k = 0.0220$  eV (right panel). We consider  $|\mu_1| = 1$  and choices for  $\lambda = |y_1|^2/|y_2|^2 = 0.01$  (orange line), 0.1 (magenta line) and 1 (red line) in both panels are shown. Since  $k$  (see Table 3) does not change much with the change of  $\delta$ , correlation between  $v_f$  and  $\Lambda$  remains almost unaltered as seen from the two panels of Fig. 12. The dotted section of each contour line in Fig. 12 represents the excluded part in view of Eq. (5.8). With some specific choices of  $C_1$  (satisfying Eq. (5.7)) we have listed the corresponding scale  $\Lambda$  in Table 7.

### 5.1.3 Case C: [ $\phi_{da} = 0$ ]

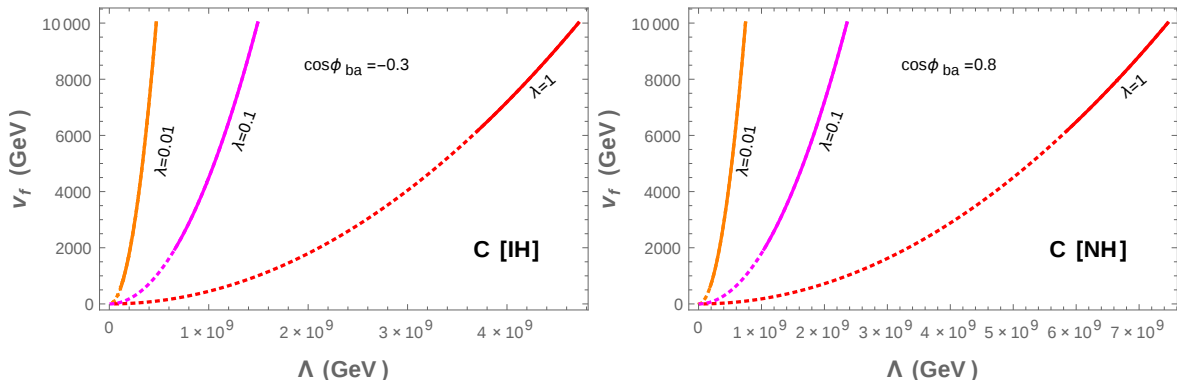


Figure 13: [Left panel] Contour plot for  $k = 0.0544$  eV in the  $v_f - \Lambda$  plane for  $\phi_{da} = 0$  and  $\cos\phi_{ba} = -0.3$  ( $\alpha = 0.814$ ) [IH: Inverted hierarchy]. [Right panel] Contour plot for  $k = 0.0218$  GeV in the  $v_f - \Lambda$  plane for  $\phi_{ba} = 0$  and  $\cos\phi_{ba} = 0.8$  ( $\alpha = 1.904$ ) [NH: Normal hierarchy]. In both the panels orange, magenta and red lines stand for  $\lambda = 0.01, 0.1$  and 1 respectively.

In this case, as we conclude from Fig. 4, the range of  $\alpha$  is restricted as  $0.478 < \alpha < 0.863$  for  $\cos\phi_{ba} < 0$  and  $1.247 < \alpha < 2.162$  for  $\cos\phi_{ba} > 0$ . We have found that  $\cos\phi_{ba} < 0$  represents inverted hierarchy while  $\cos\phi_{ba} > 0$  stands for normal hierarchy. Here  $\delta$  turns out to be zero. Therefore for a specific value of  $\alpha$  (and hence also for  $\cos\phi_{ba}$ ) we obtain the corresponding value of  $k$  as mentioned in Table 4. Using that particular  $k$ , we draw contour plot of  $k$  in  $v_f$ - $\Lambda$  plane in Fig. 13 where Eq. (5.9) is employed. Left panel of Fig. 13 is for inverted hierarchy of light neutrinos and right panel represents the case of normal hierarchy. Using the non-unitarity constraints through Eq. (5.8), similar to Case A and Case B, here

also we indicate the disallowed portion of  $v_f$ - $\Lambda$  correlation. Considering some specific choice of  $C_1$ , we provide sample values of  $\Lambda$  in Table 8.

	$C_1 = 7.5 \times 10^{-4}$			$C_1 = 4 \times 10^{-4}$		
	$\lambda = 0.01$	$\lambda = 0.1$	$\lambda = 1$	$\lambda = 0.01$	$\lambda = 0.1$	$\lambda = 1$
$\Lambda$ in GeV ( $\cos \phi_{ba} = -0.3$ )	$1.19 \times 10^8$	$6.69 \times 10^8$	$3.76 \times 10^9$	$1.40 \times 10^8$	$7.82 \times 10^8$	$4.40 \times 10^9$
$\Lambda$ in GeV ( $\cos \phi_{ba} = 0.8$ )	$1.88 \times 10^8$	$1.06 \times 10^9$	$5.94 \times 10^9$	$2.20 \times 10^8$	$1.24 \times 10^9$	$6.95 \times 10^8$

Table 8: Cutoff scale  $\Lambda$  for different  $C_1$  and  $\cos \phi_{ba}$  (with  $\phi_{da} = 0$ ) when  $\lambda = 0.01, 0.1$  and  $1$ .

#### 5.1.4 Case D: [ $\phi_{ba} = \phi_{da} = \phi$ ]

With the consideration  $\phi_{ba} = \phi_{da} = \phi$ , we have already discussed in the previous section that  $\alpha, \beta \sin \theta_{13}$  and  $r$  are correlated with the choice of  $\delta$ . We have listed  $\alpha, \beta$  as well as  $k$  for different allowed values of  $\delta$  in Table 5. As discussed before, here also we can plot the dependency of  $v_f - \Lambda$  using Eq. (5.9) and estimate the allowed regions for  $v_f$  and  $\Lambda$  employing Eq. (5.8). In Fig. 14 we have plotted this dependency for various choice of  $\lambda$  with  $\delta = 30^\circ$  (left panel) and  $\delta = 60^\circ$  (right panel). In both of these panels orange, magenta and red lines stand for  $\lambda = 0.01, 0.1$  and  $1$  respectively. Following this we have listed few representative values of  $\Lambda$  in Table 9.

	$C_1 = 7.5 \times 10^{-4}$			$C_1 = 4 \times 10^{-4}$		
	$\lambda = 0.01$	$\lambda = 0.1$	$\lambda = 1$	$\lambda = 0.01$	$\lambda = 0.1$	$\lambda = 1$
$\Lambda$ in GeV ( $\delta = 30^\circ$ )	$1.68 \times 10^8$	$9.48 \times 10^8$	$5.30 \times 10^9$	$1.96 \times 10^8$	$1.10 \times 10^9$	$6.20 \times 10^9$
$\Lambda$ in GeV ( $\delta = 60^\circ$ )	$1.08 \times 10^8$	$6.08 \times 10^8$	$3.42 \times 10^9$	$1.26 \times 10^8$	$7.11 \times 10^8$	$4.00 \times 10^9$

Table 9: Cutoff scale  $\Lambda$  for different  $C_1$  and  $\delta$  (with  $\phi_{ba} = \phi_{da} = \phi$ ) when  $\lambda = 0.01, 0.1$  and  $1$ .

#### 5.1.5 General Case

From our previous analysis in section 4, we choose a particular value of  $\delta = 260^\circ$  for this general case (a value close to recent hint [9–12]) to study the scales  $v_f, \Lambda$ . The set of parameters that would correspond to this value of  $\delta$  are found to be  $\alpha = 2.25, \beta = 1, \phi_{ba} = 0.5$  and  $\phi_{da} = 2$  which satisfy constraints imposed from mixing angles,  $r$  and  $\sum m_i < 0.23$  eV. Here  $k$  is found to be  $0.0147$  eV in order to have adequate solar and atmospheric splittings. Using this  $k$  through Eq. (5.9), we then obtain the contour plot of  $v_f$  against  $\lambda$  as shown in Fig. 15 for different choices of  $\lambda$ . The dotted portion in each curve indicates the excluded part in view of Eq. (5.8) with  $C_1 = 7.5 \times 10^{-4}$  (left panel) and  $C_1 = 4 \times 10^{-4}$  (right panel). These numerical estimates are summarized in Table 10.

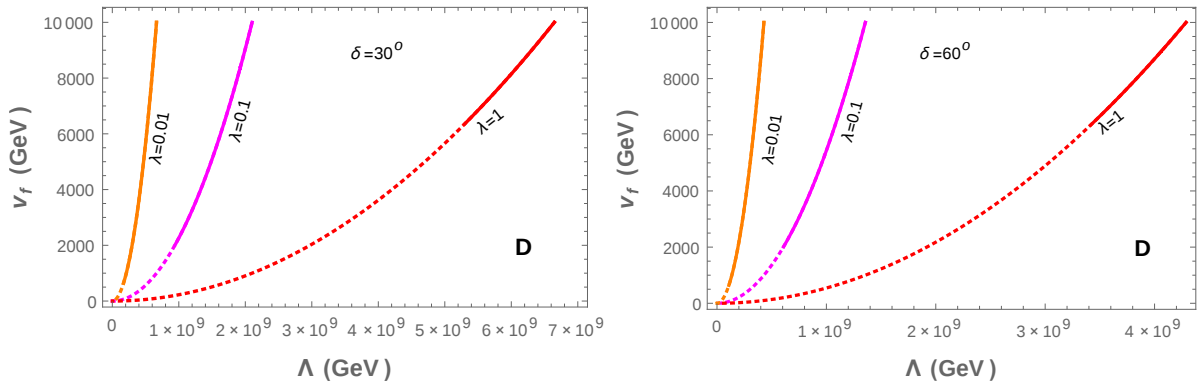


Figure 14: [Left panel] Contour plot for  $k = 0.0274$  eV in the  $v_f - \Lambda$  plane for  $\phi_{ba} = \phi_{da} = \phi$  and  $\delta = 30^\circ$ . [Right panel] Contour plot for  $k = 0.0658$  eV in the  $v_f - \Lambda$  plane for  $\phi_{ba} = \phi_{da} = \phi$  and  $\delta = 60^\circ$ . In both the panels orange, magenta and red lines stand for  $\lambda = 0.01, 0.1$  and  $1$  respectively.

	$\lambda = 0.01$	$\lambda = 0.1$	$\lambda = 1$
$\Lambda$ in GeV (for $C_1 = 7.5 \times 10^{-4}$ )	$2.29 \times 10^8$	$1.28 \times 10^9$	$7.22 \times 10^9$
$\Lambda$ in GeV (for $C_1 = 4 \times 10^{-4}$ )	$2.68 \times 10^8$	$1.50 \times 10^9$	$8.45 \times 10^9$

Table 10: Cutoff scale  $\Lambda$  for different  $C_1$  with  $\delta = 260^\circ$  (with  $\alpha = 2.25, \beta = 1, \phi_{ba} = 0.5$  and  $\phi_{da} = 2$ ) and  $\lambda = 0.01, 0.1$  and  $1$ .

## 5.2 Lepton flavor violation

In view of the presence of this non-unitarity effect, the neutrino states ( $\nu_{\alpha L}$  with  $\alpha = e, \mu, \tau$ ) appearing in the SM charged current interaction Lagrangian now can be written as,

$$\nu_{\alpha L} = [(1 - C_1) U_\nu]_{\alpha i} \nu_i + [\mathcal{K}]_{\alpha j} N_j, \quad (5.10)$$

where the matrix  $W_{3 \times 6}$  (see Eq. (5.4)) is conventionally denoted by  $\mathcal{K}$ .  $\nu_{i=1,2,3}$  and  $N_{j=4,5,\dots,9}$  are the light and heavy neutrino mass eigenstates respectively. Then in a basis where charged leptons are diagonal (as in our case), the charged current interactions have contributions involving three light neutrinos  $\nu_i$  and six heavy neutrinos  $N_j$  as

$$-\mathcal{L}_{CC} = \frac{g}{\sqrt{2}} \bar{l}_\alpha \gamma^\mu \{ [(1 - C_1) U_\nu]_{\alpha i} \nu_i + [\mathcal{K}]_{\alpha j} N_j \} W_\mu^- + \text{h.c.} \quad (5.11)$$

These nine neutrino states can therefore mediate lepton flavor violating decays like  $l_\alpha \rightarrow l_\beta \gamma$  in one loop (e.g.  $\mu \rightarrow e \gamma$ ). Resulting branching ratio for such processes (in the limit  $m_\beta \rightarrow 0$ ) now can be written as [42, 43, 45–51],

$$\text{BR}(L_\alpha \rightarrow L_\beta \gamma) \simeq \frac{\alpha_W^3 \sin^2 \theta_W m_{l_\alpha}^5}{256 \pi^2 m_W^4 \Gamma_{l_\alpha}} \left| \sum_{j=1}^3 [(1 - C_1) U_\nu]_{\alpha j}^* [(1 - C_1) U_\nu]_{\beta k j} I_\gamma \left( \frac{m_{\nu_j}^2}{m_W^2} \right) + \sum_{l=4}^9 \mathcal{K}_{\alpha l}^* \mathcal{K}_{\beta l} I_\gamma \left( \frac{m_{N_l}^2}{m_W^2} \right) \right|^2, \quad (5.12)$$



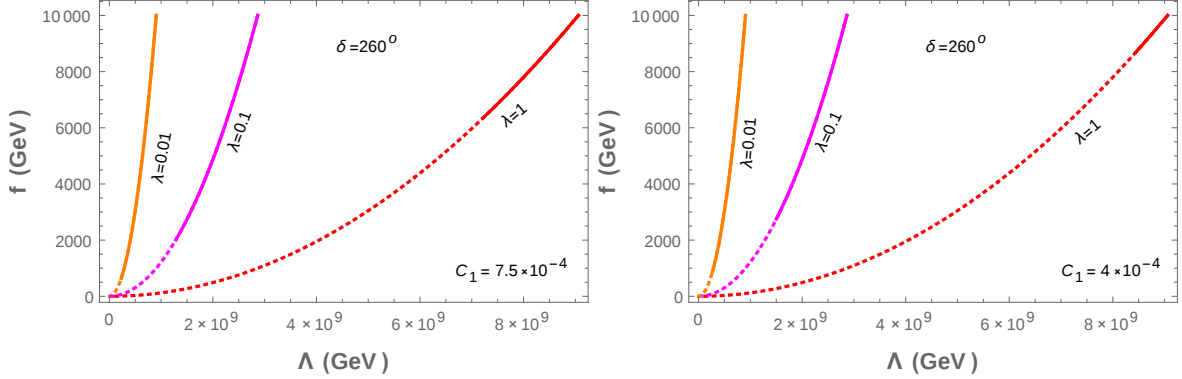


Figure 15: Contour plot for  $k = 0.0147$  eV in the  $\nu_f - \Lambda$  plane where  $\alpha = 2.25, \beta = 1, \phi_{ba} = 0.5$  and  $\phi_{da} = 2$  and with  $C_1 = 7.5 \times 10^{-4}$  (left panel) and  $C_1 = 4 \times 10^{-4}$  (right panel). In both the panels orange, magenta and red lines stand for  $\lambda = 0.01, 0.1$  and  $1$  respectively.

where

$$I_\gamma(x) = \frac{10 - 43x + 78x^2 - 49x^3 + 18x^3 \ln x + 4x^4}{12(1-x)^4}, \quad \text{with } x = \frac{m_{\nu,N}^2}{m_W^2}. \quad (5.13)$$

Here  $\alpha_W = g^2/4\pi$ , with  $g$  as the weak coupling,  $\theta_W$  is electroweak mixing angle,  $m_W$  is  $W^\pm$  boson mass and  $\Gamma_{l_\alpha}$  is the total decay width of the decaying charged lepton  $l_\alpha$ . Current upper bound for the branching ratio of the LFV decays are [30] (at 90% CL)

$$\text{BR}(\mu \rightarrow e\gamma) < 5.7 \times 10^{-13}, \quad (5.14)$$

$$\text{BR}(\tau \rightarrow e\gamma) < 3.3 \times 10^{-8}, \quad (5.15)$$

$$\text{BR}(\tau \rightarrow \mu\gamma) < 4.4 \times 10^{-8}. \quad (5.16)$$

Another important lepton flavor violating decay  $\mu \rightarrow eee$  is also worthy to mention and details of computation of branching ratio calculation can be found in [42, 43]. Current upper limit for this decay is  $\text{BR}(\mu \rightarrow eee) < 1.0 \times 10^{-12}$  (90% CL) [30].

Since the flavor structure of the neutrino mass matrix is already fixed in our present scenario (from the  $A_4$  and additional symmetry consideration), it would provide some concrete understanding for the LFV processes in this inverse seesaw model. Both the  $W_{3 \times 3} = (1 - C_1)U_\nu$  and  $W_{3 \times 6} = \mathcal{K}$  matrices play the instrumental role here. Remember that,  $U_\nu$  is the diagonalizing matrix for the light neutrinos, defined by  $U_\nu = U_{TB}U_1U_m$  as discussed in section 3. Hence this can be obtained in terms of  $\alpha, \beta, k, \phi_{ba}$  and  $\phi_{da}$ . The non-unitary parameter  $C_1$  is required to satisfy,  $C_1 = \lambda v^2/2v_f^2 < 8 \times 10^{-4}$  as discussed earlier. Therefore we can completely evaluate  $W_{3 \times 3} = (1 - C_1)U_\nu$ , once a specific value of  $C_1$  is chosen.

On the other hand the rectangular matrix  $\mathcal{K}$  is approximately given by [40, 41]

$$\mathcal{K} \simeq (-F\mu M^{-1}, F)U_h, \quad (5.17)$$

where  $U_h$  is the diagonalizing matrix of  $m_{\nu_{heavy}}$  given in Eq. (5.2). As previously mentioned,  $F = m_D M^{-1}$  in our scenario is proportional to identity matrix of order  $3 \times 3$ , *i.e.*  $F = \frac{y_1 v}{y_2 v_f} \mathbb{I}_{3 \times 3} = f_1 \mathbb{I}_{3 \times 3}$ . Hence, the matrix  $\mathcal{K}$  turns out to be

$$\mathcal{K} = (-f_1 \mu M^{-1}, f_1 \mathbb{I}_{3 \times 3}) U_h. \quad (5.18)$$

Using Eqs. (2.4) and (2.5), we find

$$\mu M^{-1} = \frac{a}{y_2 v_f} \begin{pmatrix} 1 - \frac{2}{3} \alpha e^{i\phi_{ba}} & \frac{1}{3} \alpha e^{i\phi_{ba}} + \beta e^{i\phi_{da}} & \frac{1}{3} \alpha e^{i\phi_{ba}} \\ \frac{1}{3} \alpha e^{i\phi_{ba}} & 1 + \frac{1}{3} \alpha e^{i\phi_{ba}} & -\frac{2}{3} \alpha e^{i\phi_{ba}} + \beta e^{i\phi_{da}} \\ \frac{1}{3} \alpha e^{i\phi_{ba}} + \beta e^{i\phi_{da}} & -\frac{2}{3} \alpha e^{i\phi_{ba}} & 1 + \frac{1}{3} \alpha e^{i\phi_{ba}} \end{pmatrix}, \quad (5.19)$$

where we have used the explicit flavor structure of  $\mu$  and  $M$ .

We now proceed to find out the form of  $U_h$ , the diagonalizing matrix of  $m_{\nu_{heavy}}$ . Note that the  $m_{\nu_{heavy}}$  matrix can first be block diagonalized by  $V_0$  as

$$m'_{\nu_{heavy}} = (V_0)^T m_{\nu_{heavy}} V_0 \simeq \begin{pmatrix} -M + \mu/2 & 0 \\ 0 & M + \mu/2 \end{pmatrix}, \quad (5.20)$$

where  $V_0$  is given by (in our scenario both  $\mu$  and  $M$  are symmetric matrices)

$$V_0 \simeq \frac{1}{\sqrt{2}} \begin{pmatrix} \mathbb{I} + \frac{\mu M^{-1}}{4} & \mathbb{I} - \frac{\mu M^{-1}}{4} \\ -\mathbb{I} + \frac{\mu M^{-1}}{4} & \mathbb{I} + \frac{\mu M^{-1}}{4} \end{pmatrix}. \quad (5.21)$$

Here we have neglected the terms involving higher orders in  $\mu M^{-1}$  as expected in inverse seesaw scenario in general. Now the upper  $(-M + \mu/2)$  and lower  $(M + \mu/2)$  block matrices of  $m'_{\nu_{heavy}}$  carry the form of  $\mu$  matrix itself (or  $m_\nu$ ). The presence of  $M$  just redefines the previous parameter  $a$  by  $a_{1,2} = a/2 \mp y_2 v_f$  (see Eq. (2.4) and (2.5)). Therefore we can follow the similar prescription for diagonalizing these blocks as we did in case of  $m_\nu$  diagonalization. Hence  $m'_{\nu_{heavy}}$  can further be diagonalized by  $V^T m'_{\nu_{heavy}} V$  with

$$V = \begin{pmatrix} U_{TB} \cdot V_1(\theta_1, \psi_1) & 0 \\ 0 & U_{TB} \cdot V_2(\theta_2, \psi_2) \end{pmatrix}, \quad (5.22)$$

where  $V_i$  has the form similar to  $U_1$ , *i.e.*

$$V_i = \begin{pmatrix} \cos \theta_i & 0 & \sin \theta_i e^{-i\psi_i} \\ 0 & 1 & 0 \\ -\sin \theta_i e^{i\psi_i} & 0 & \cos \theta_i \end{pmatrix}. \quad (5.23)$$

Therefore the diagonalizing matrix of  $m_{\nu_{heavy}}$  can be written as

$$U_h \simeq \frac{1}{\sqrt{2}} \begin{pmatrix} \mathbb{I} + \frac{\mu M^{-1}}{4} & \mathbb{I} - \frac{\mu M^{-1}}{4} \\ -\mathbb{I} + \frac{\mu M^{-1}}{4} & \mathbb{I} + \frac{\mu M^{-1}}{4} \end{pmatrix} \begin{pmatrix} U_{TB} \cdot V_1(\theta_1, \psi_1) & 0 \\ 0 & U_{TB} \cdot V_2(\theta_2, \psi_1) \end{pmatrix}. \quad (5.24)$$

In order to find  $U_h$ , we use  $\mu M^{-1}$  as obtained in Eq. (5.19). Furthermore, we get  $\theta_{1,2}$  and  $\psi_{1,2}$  appearing in  $V_{1,2}$  as discussed earlier. Hence following the same way as in Eq. (3.8) and Eq. (3.9) we find

$$\tan 2\theta_i = \frac{\sqrt{3}\beta_i \cos \phi_{da}}{(\beta_i \cos \phi_{da} - 2) \cos \psi_i + 2\alpha_i \sin \phi_{ba} \sin \psi_i}, \quad (5.25)$$

$$\tan \psi_i = \frac{\sin \phi_{da}}{\alpha_i \cos(\phi_{ba} - \phi_{da})}, \quad (5.26)$$

with  $i = 1, 2$  and we use the definition of  $\alpha_i$  and  $\beta_i$  as,

$$\alpha_{1,2} = \frac{|b|}{|a| \mp 2|y_2|v_f} \text{ and } \beta_{1,2} = \frac{|d|}{|a| \mp 2|y_2|v_f}. \quad (5.27)$$

For simplicity we discard phase difference between  $y_2$  and  $a$ , and set  $\phi_{y_2 a} = 0$ .

Note that from our understanding in Sections 3-4, we can have estimates over the parameters  $\alpha, \beta, k$  along with the phases  $\phi_{ba}, \phi_{da}$  in order to satisfy  $\sin \theta_{13}$ , other mixing angles,  $r$ , individual solar and atmospheric splittings, also to be consistent with the upper bound on sum of the light neutrino masses. Specific choice of  $C_1$  enables us to compute magnitude of the flavon vev  $v_f$  and hence  $|a|$  from Eq. (5.9). With all these values in hand we can finally evaluate parameters  $\theta_i, \psi_i, \alpha_i$  and  $\beta_i$  appearing in  $U_h$ . Here we consider <sup>6</sup>  $|y_2| = 1$ . Now following the analytic expressions in Eqs. (5.17-5.19), (5.22-5.27), we can estimate  $W_{3 \times 3}$  and  $\mathcal{K}$  and hence the corresponding contribution to the branching ratio (see Eq. (5.12)). Due to particular flavor structures of the matrices  $\mu$  as well as  $m_D$  and  $M$ , we find  $W_{3 \times 3}$  and  $\mathcal{K}$  are such that this scenario predicts vanishingly small branching ratio ( $\sim 10^{-35}$ ) for LFV decays.

In addition, we have performed the evaluation numerically also. In order to evaluate it, we need to diagonalize the entire  $9 \times 9$  neutrino mass matrix  $M_\nu$ . Since the neutrino mixings are entirely dictated by the flavor structure of  $\mu$  matrix, we could have find the entire  $M_\nu$  numerically with the choices of  $\alpha, \beta, k$  along with the phases  $\phi_{ba}, \phi_{da}$  as done in cases A, B, C, D and the general case. However to compute  $m_D$  and  $M$ , we need consider to  $|y_1|$  and  $|y_2|$  separately (for example, to have  $\lambda = 1$ , we assume  $|y_1| = |y_2| = 1$ ). Then following Eq. (2.3), we can entirely construct the  $M_\nu$  matrix numerically. Then with the help of Mathematica<sup>7</sup>, we are able to find the diagonalizing matrix  $W$  (and hence  $\mathcal{K}$  matrix also) and have estimate over the LFV decays. It turns out that the numerical estimate coincides with our analytical evaluation of vanishingly small branching ratios for LFV decays to a good extent.

---

<sup>6</sup>A common phase  $\phi_0$  as described in the discussion above Eq. (3.19) in Section 3, is irrelevant for neutrino phenomenology and hence we put it at zero. We also set phases of  $f_1$  and  $a/y_2$  to zero.

<sup>7</sup>We also use Takagi factorization [44] to find  $W$ .

### 5.3 Neutrinoless double beta decay and contribution of heavy neutrinos

We note that in addition to the standard contribution to the effective mass parameter involved in neutrinoless double beta decay as described in Section 3, there will be additional contribution due the presence of mixing between light and heavy neutrinos (*i.e.* with nonzero  $W_{3\times 6}$ ). Hence the half life associated with neutrinoless double beta can be expressed as [54, 55, 57, 58]

$$(T_{1/2}^{0\nu})^{-1} = \mathcal{G}^{0\nu} \left| \frac{\mathcal{M}_\nu}{m_e} \right|^2 \left| \sum_{i=1}^3 (W_{3\times 3})_{ei}^2 m_i + \langle q^2 \rangle \sum_{i=1}^6 (W_{3\times 6})_{ei}^2 m_N^{-1} \right|^2 \quad (5.28)$$

where  $\mathcal{G}^{0\nu}$  is the phase space factor and  $\langle q^2 \rangle = -m_e m_p \mathcal{M}_\nu / \mathcal{M}_N = -(182 \text{ MeV}^2)$  [54]. Here  $m_e$  is the mass of electron,  $m_p$  is the mass of proton,  $\mathcal{M}_\nu$  is the nuclear matrix element for light neutrino states and  $\mathcal{M}_N$  is nuclear matrix element for heavy neutrino states. Here the first and second contribution in Eq. (5.28) is due to the light and heavy neutrinos respectively. We already have an estimate for the first contribution (with  $W_{3\times 3} \simeq (1 - \eta) U_\nu$ ) as provided in several tables of Section 4, which turns out to be of order  $\sim 10^{-2}$  eV. Now with some specific choice of  $\lambda$  and  $|y_2|$ , we can determine the  $W$  matrix numerically as discussed in the previous subsection where information on other parameters  $\alpha, \beta, k$  *etc.* are taken from Section 4 (different cases). Then we evaluate numerically the  $\mathcal{K}$  (*i.e.*  $W_{3\times 6}$ ). In order to maximize this contribution, we consider lowest value of  $v_f$  which is allowed from Eq. (5.8). It turns out then that the second contribution remains sub-dominant ( $\sim 10^{-6}$  eV or less) compared to the first contribution of Eq. (5.28). The smallness of the second term can also be understood from our finding for  $\mathcal{K}$  as  $\mathcal{K}_{ei} = f(U_h)_{4i}$ . A naive estimate for this contribution (to  $|m_{ee}|$ ) therefore is of order  $\frac{\lambda}{y_2} v^2 \langle q^2 \rangle / v_f^3$ . The using the lowest possible  $v_f$  consistent with Eq. (5.8), the estimate indicates that this contribution is essentially small compared to the first contribution. So the effective mass involved in the neutrinoless double beta decay process is mostly unaffected with the presence of heavy neutrinos in the present set-up.

## 6 Conclusion

We have considered an inverse seesaw framework embedded in a flavor symmetric environment in order to study whether it can accommodate the neutrino masses and mixing as suggested from present experimental data, particularly in view of nonzero  $\theta_{13}$ . We employ an  $A_4 \times Z_4 \times Z_3$  discrete symmetry which is concocted with a global  $B - L$  symmetry. We note that the flavor structure of light neutrino mass matrix is essentially dictated by that of the  $\mu$  matrix itself, which is the matrix containing the lepton number breaking contribution in the inverse seesaw scenario. The flavor structure of  $\mu$  matrix is generated when the flavons have vevs. We notice that the typical structure of this matrix can lead to a lepton mixing consistent with neutrino

data where the charged lepton mass matrix is found to be diagonal in the framework. In doing this analysis, we have studied the correlation between different parameters of the model and their dependence on the neutrino parameters such as mass-squared differences, mixing angles etc., evaluated from experimental results. Dependency on the Dirac CP violating phase is also studied.

Since there exists a small mixing between light and heavy neutrino states in the framework, we have also checked the non-unitarity effects in our set-up which contribute to LFV processes, neutrinoless double beta decay etc.. We have found that owing to the typical flavor structure of the neutrino mass matrix here, the effective contribution of it to the LFV processes and neutrinoless double beta decays are vanishingly small. It can be noted that the  $\mu$  matrix results from the breaking of a flavon which carries charge under the global  $U(1)_{B-L}$ . Hence we expect to have Goldstone boson or majoron ( $J$ ) [56]. It may open Higgs boson decay channel ( $H \rightarrow JJ$ ) and demands extensive analysis in the context of current and future LHC data. Discussions in this direction can be found in [52, 53]. Particularly current 13 TeV run of LHC will be important for such analysis. However further discussion in this regard is beyond the scope of the present study. Since the new physics scale in the present set-up is around few TeV, collider aspects of such a scenario turns out to be interesting and discussion in this direction can be found in [59, 60].

## Appendix

### A VEV alignments of flavons

The most general renormalizable potential involving all the flavons of our set-up which is invariant under  $A_4 \times Z_4 \times Z_3$  and respecting  $U(1)_{B-L}$  can be written as

$$V = V(H) + V(\phi_S) + V(\phi_T) + V(\xi) + V(\xi') + V(\rho) + V(H, \phi_S, \phi_T, \xi, \xi', \rho) + V(\phi_S, \phi_T, \xi, \xi', \rho)$$

where

$$V(H) = \mu_H^2 H^\dagger H + \lambda_H (H^\dagger H)(H^\dagger H) \quad (\text{A.1})$$

$$\begin{aligned} V(\phi_S) = & \mu_S^2 (\phi_S^\dagger \phi_S)_1 + \lambda_1^S (\phi_S^\dagger \phi_S)_1 (\phi_S^\dagger \phi_S)_1 + \lambda_2^S (\phi_S^\dagger \phi_S)_{1'} (\phi_S^\dagger \phi_S)_{1''} \\ & \lambda_3^S (\phi_S^\dagger \phi_S)_{3S} (\phi_S^\dagger \phi_S)_{3S} + \lambda_4^S (\phi_S^\dagger \phi_S)_{3A} (\phi_S^\dagger \phi_S)_{3A} \\ & + \lambda_5^S (\phi_S^\dagger \phi_S)_{3S} (\phi_S^\dagger \phi_S)_{3A} \end{aligned} \quad (\text{A.2})$$

$$\begin{aligned}
V(\phi_T) &= \mu_T^2(\phi_T^\dagger\phi_T)_1 + \lambda_T^1(\phi_T^\dagger\phi_T)_1(\phi_T^\dagger\phi_T)_1 + \lambda_T^2(\phi_T^\dagger\phi_T)_{1'}(\phi_T^\dagger\phi_T)_{1''} \\
&\quad + \lambda_T^3(\phi_T^\dagger\phi_T)_{3S}(\phi_T^\dagger\phi_T)_{3S} + \lambda_T^4(\phi_T^\dagger\phi_T)_{3A}(\phi_T^\dagger\phi_T)_{3A} \\
&\quad + \lambda_T^4(\phi_T^\dagger\phi_T)_{3S}(\phi_T^\dagger\phi_T)_{3A} \tag{A.3}
\end{aligned}$$

$$V(\xi) = \mu_\xi^2\xi^\dagger\xi + \lambda_\xi(\xi^\dagger\xi)(\xi^\dagger\xi) \tag{A.4}$$

$$V(\xi') = \mu_{\xi'}^2\xi'^\dagger\xi' + \lambda_{\xi'}(\xi'^\dagger\xi')(\xi'^\dagger\xi') \tag{A.5}$$

$$V(\rho) = \mu_\rho^2\rho^\dagger\rho + \lambda_\rho(\rho^\dagger\rho)(\rho^\dagger\rho) \tag{A.6}$$

$$\begin{aligned}
V(H, \phi_S, \phi_T, \xi, \xi', \rho) &= \lambda_{HS}(H^\dagger H)(\phi_S^\dagger\phi_S)_1 + \lambda_{HT}(H^\dagger H)(\phi_T^\dagger\phi_T)_1 \\
&\quad + \lambda_{H\xi}(H^\dagger H)(\xi^\dagger\xi) + \lambda_{H\rho}(H^\dagger H)(\rho^\dagger\rho) + \lambda_{H\xi'}(H^\dagger H)(\xi'^\dagger\xi') \tag{A.7}
\end{aligned}$$

$$\begin{aligned}
V(\phi_S, \phi_T, \xi, \xi', \rho) &= k_{11}(\phi_T\phi_T)_{3S}\phi_T + k_{12}(\phi_T\phi_T)_{3A}\phi_T + k_{31}(\phi_S^\dagger\phi_S)_{3S}\phi_T + k_{32}(\phi_S^\dagger\phi_S)_{3A}\phi_T \\
&\quad + k_4(\phi_S\phi_T)_1\xi^\dagger + k_5(\phi_S\phi_T)_{1'}\xi'^\dagger + k_6(\phi_S^\dagger\phi_T)_1\xi + k_7(\phi_S^\dagger\phi_T)_{1''}\xi' \\
&\quad + k_8(\phi_S\phi_T^\dagger)_1\xi^\dagger + k_9(\phi_S\phi_T^\dagger)_{1'}\xi'^\dagger + k_{10}(\phi_S^\dagger\phi_T^\dagger)_1\xi + k'_{10}(\phi_S^\dagger\phi_T^\dagger)_{1''}\xi' \\
&\quad + \lambda_{ST}^1(\phi_S^\dagger\phi_S)_1(\phi_T^\dagger\phi_T)_1 + \lambda_{ST}^2(\phi_S^\dagger\phi_S)_{1'}(\phi_T^\dagger\phi_T)_{1''} \\
&\quad + \lambda_{ST}^{22}(\phi_S^\dagger\phi_S)_{1''}(\phi_T^\dagger\phi_T)_{1'} + \lambda_{ST}^3(\phi_S^\dagger\phi_S)_{3S}(\phi_T^\dagger\phi_T)_{3S} \\
&\quad + \lambda_{ST}^4(\phi_S^\dagger\phi_S)_{3A}(\phi_T^\dagger\phi_T)_{3A} + \lambda_{ST}^5(\phi_S^\dagger\phi_S)_{3S}(\phi_T^\dagger\phi_T)_{3A} \\
&\quad + \lambda_{ST}^6(\phi_S^\dagger\phi_S)_{3A}(\phi_T^\dagger\phi_T)_{3S} + \lambda_{ST}^1(\phi_S^\dagger\phi_T)_1(\phi_T^\dagger\phi_S)_1 \\
&\quad + \lambda_{ST}^2(\phi_S^\dagger\phi_T)_{1'}(\phi_T^\dagger\phi_S)_{1''} + \lambda_{ST}^{22}(\phi_S^\dagger\phi_T)_{1''}(\phi_T^\dagger\phi_S)_{1'} \\
&\quad + \lambda_{ST}^3(\phi_S^\dagger\phi_T)_{3S}(\phi_T^\dagger\phi_S)_{3S} + \lambda_{ST}^4(\phi_S^\dagger\phi_T)_{3A}(\phi_T^\dagger\phi_S)_{3A} \\
&\quad + \lambda_{ST}^5(\phi_S^\dagger\phi_T)_{3S}(\phi_T^\dagger\phi_S)_{3A} + \lambda_{ST}^6(\phi_S^\dagger\phi_T)_{3A}(\phi_T^\dagger\phi_S)_{3S} \\
&\quad + \lambda_{S\xi}(\phi_S^\dagger\phi_S)_1(\xi^\dagger\xi) + \lambda'_{S\xi}(\phi_S^\dagger\xi)(\xi^\dagger\phi_S) \\
&\quad + \lambda_{S\xi'}(\phi_S^\dagger\phi_S)_1(\xi'^\dagger\xi') + \lambda'_{S\xi'}(\phi_S^\dagger\xi')(\xi'^\dagger\phi_S) \\
&\quad + \lambda_{S\rho}(\phi_S^\dagger\phi_S)_1(\rho^\dagger\rho) + \lambda'_{S\rho}(\phi_S^\dagger\rho)(\rho^\dagger\phi_S) \\
&\quad + \lambda_{T\xi}(\phi_T^\dagger\phi_T)_1(\xi^\dagger\xi) + \lambda'_{T\xi}(\phi_T^\dagger\xi)(\xi^\dagger\phi_T) \\
&\quad + \lambda_{T\xi'}(\phi_T^\dagger\phi_T)_1(\xi'^\dagger\xi') + \lambda'_{T\xi'}(\phi_T^\dagger\xi')(\xi'^\dagger\phi_T) \\
&\quad + \lambda_{T\rho}(\phi_T^\dagger\phi_T)_1(\rho^\dagger\rho) + \lambda'_{T\rho}(\phi_T^\dagger\rho)(\rho^\dagger\phi_T) \\
&\quad + \lambda_{\xi\rho}(\xi^\dagger\xi)(\rho^\dagger\rho) + \lambda'_{\xi\rho}(\xi^\dagger\rho)(\rho^\dagger\xi) + \lambda_{\xi\xi'}(\xi\xi^\dagger)_1(\xi'\xi'^\dagger)_1 \\
&\quad + \lambda_{\xi'\rho}(\xi'\xi'^\dagger)(\rho^\dagger\rho) + \lambda'_{\xi'\rho}(\xi'\rho^\dagger)(\xi'^\dagger\rho) \\
&\quad + \lambda_{S\xi\xi'}(\phi_S^\dagger\phi_S)_{1''}(\xi^\dagger\xi')_{1'} + \lambda_{T\xi\xi'}(\phi_T^\dagger\phi_T)_{1''}(\xi^\dagger\xi')_{1'}
\end{aligned}$$

$$\begin{aligned}
& +\lambda_{S\xi\xi'}^2(\phi_S^\dagger\phi_S)_{1'}(\xi\xi'^\dagger)_{1''} + \lambda_{T\xi\xi'}^2(\phi_T^\dagger\phi_T)_{1'}(\xi\xi'^\dagger)_{1''} \\
& +\lambda_{SS\xi}^1(\phi_S^\dagger\phi_S)_{3S}(\phi_S\xi^\dagger) + \lambda_{SS\xi}^2(\phi_S^\dagger\phi_S)_{3A}(\phi_S\xi^\dagger) \\
& +\lambda_{SS\xi'}^1(\phi_S^\dagger\phi_S)_{3S}(\phi_S\xi'^\dagger) + \lambda_{SS\xi'}^2(\phi_S^\dagger\phi_S)_{3A}(\phi_S\xi'^\dagger) \\
& +\lambda_{TS\xi}^1(\phi_T^\dagger\phi_T)_{3S}(\phi_S\xi^\dagger) + \lambda_{TS\xi}^2(\phi_T^\dagger\phi_T)_{3A}(\phi_S\xi^\dagger) \\
& +\lambda_{TS\xi'}^1(\phi_T^\dagger\phi_T)_{3S}(\phi_S\xi'^\dagger) + \lambda_{TS\xi'}^2(\phi_T^\dagger\phi_T)_{3A}(\phi_S\xi'^\dagger) \\
& +\lambda_{SS\xi}^{11}(\phi_S^\dagger\phi_S)_{3S}(\phi_S^\dagger\xi) + \lambda_{SS\xi}^{22}(\phi_S^\dagger\phi_S)_{3A}(\phi_S^\dagger\xi) \\
& +\lambda_{SS\xi'}^{11}(\phi_S^\dagger\phi_S)_{3S}(\phi_S^\dagger\xi') + \lambda_{SS\xi'}^{22}(\phi_S^\dagger\phi_S)_{3A}(\phi_S^\dagger\xi') \\
& +\lambda_{TS\xi}^{11}(\phi_T^\dagger\phi_T)_{3S}(\phi_S^\dagger\xi) + \lambda_{TS\xi}^{22}(\phi_T^\dagger\phi_T)_{3A}(\phi_S^\dagger\xi) \\
& +\lambda_{TS\xi'}^{11}(\phi_T^\dagger\phi_T)_{3S}(\phi_S^\dagger\xi') + \lambda_{TS\xi'}^{22}(\phi_T^\dagger\phi_T)_{3A}(\phi_S^\dagger\xi'). \tag{A.8}
\end{aligned}$$

Here the explicit multiplication of  $A_4$  are taken into account. In general this potential involves several free parameters. These plenty free parameters should naturally allow therefore the required vev alignment of the flavons we considered,  $\langle\phi_S\rangle = v_S(1, 1, 1)$ ,  $\langle\phi_T\rangle = v_T(1, 0, 0)$ ,  $\langle\xi\rangle = v_\xi$ ,  $\langle\xi'\rangle = v_{\xi'}$ ,  $\langle\rho\rangle = v_\rho$ . For example, with a particular choice like the followings<sup>8</sup>

$$\begin{aligned}
& [3\lambda_{HS}v^2 + 3\lambda_{HT}v^2 + \lambda_{H\xi}v^2 + \lambda_{H\xi'}v^2 + \lambda_{H\rho}v^2 - 3\mu_S^2 - 3\mu_T^2 - \mu_\xi^2 - \mu_{\xi'}^2 - \mu_\rho^2] \sim 1 \text{ GeV}^2 \\
& [2k_{11} + k_4 + k_5 + k_6 + k_7 + k_8 + k_9 + k_{10} + k'_{10}] \sim -1 \text{ GeV} \\
& [9(\lambda_1^S + \lambda_2^S) + (3\lambda_{ST}^1 + \lambda_{ST}^{22} + \lambda_{ST}^1 + \lambda_{ST}^2 + \lambda_{ST}^{22} + 6\lambda_{ST}^3 + 2\lambda_{ST}^4) + \\
& \quad (3\lambda_{S\xi} + 3\lambda'_{S\xi}) + (3\lambda_{S\xi'} + 3\lambda'_{S\xi'}) + (9\lambda_1^T + 4\lambda_3^T) + (3\lambda_{S\rho} + 3\lambda'_{S\rho}) \\
& \quad (\lambda_{\xi\rho} + \lambda'_{\xi\rho}) + \lambda_\rho + (\lambda_{T\xi'} + \lambda'_{T\xi'}) + (\lambda_{\xi'\rho} + \lambda'_{\xi'\rho}) + 2\lambda_{TS\xi}^{11} + 3\lambda_{S\xi\xi'}^2] \sim 0.00075.
\end{aligned}$$

can actually lead to a common vev  $v_S = v_T = v_\xi = v_{\xi'} = v_\rho \sim 1 \text{ TeV}$  along the required direction.

## References

- [1] P. Minkowski, Phys. Lett. B **67**, 421 (1977).
- [2] M. Gell-Mann, P. Ramond and R. Slansky, Conf. Proc. C **790927**, 315 (1979) [arXiv:1306.4669 [hep-th]].
- [3] R. N. Mohapatra and G. Senjanovic, Phys. Rev. Lett. **44**, 912 (1980).

<sup>8</sup>Along the specified vev directions, terms involving the couplings  $\lambda_{3,4,5}^S$ ,  $\lambda_{2,4,5}^T$ ,  $k_{12,31,32}$ ,  $\lambda_{ST}^2$ ,  $\lambda_{ST}^{22}$ ,  $\lambda_{ST}^3$ ,  $\lambda_{ST}^4$ ,  $\lambda_{ST}^5$ ,  $\lambda_{ST}^6$ ,  $\lambda_{ST}^5$ ,  $\lambda_{ST}^6$ ,  $\lambda_{T\xi'}^1$ ,  $\lambda_{T\xi'}^2$ ,  $\lambda_{T\xi'}^1$ ,  $\lambda_{T\xi'}^2$ ,  $\lambda_{SS\xi}^1$ ,  $\lambda_{SS\xi}^2$ ,  $\lambda_{SS\xi'}^1$ ,  $\lambda_{SS\xi'}^2$ ,  $\lambda_{TS\xi}^1$ ,  $\lambda_{TS\xi'}^1$ ,  $\lambda_{TS\xi'}^2$ ,  $\lambda_{SS\xi}^{11}$ ,  $\lambda_{SS\xi}^{22}$ ,  $\lambda_{SS\xi'}^{11}$ ,  $\lambda_{SS\xi'}^{22}$ ,  $\lambda_{TS\xi}^{11}$ ,  $\lambda_{TS\xi}^{22}$ ,  $\lambda_{TS\xi'}^{11}$  and  $\lambda_{TS\xi'}^{22}$  do not contribute.

- [4] R. N. Mohapatra, Phys. Rev. Lett. **56**, 561 (1986).
- [5] R. N. Mohapatra and J. W. F. Valle, Phys. Rev. D **34**, 1642 (1986).
- [6] Y. Abe *et al.* [Double Chooz Collaboration], Phys. Rev. Lett. **108**, 131801 (2012) [arXiv:1112.6353 [hep-ex]].
- [7] F. P. An *et al.* [Daya Bay Collaboration], Phys. Rev. Lett. **108**, 171803 (2012) [arXiv:1203.1669 [hep-ex]].
- [8] J. K. Ahn *et al.* [RENO Collaboration], Phys. Rev. Lett. **108**, 191802 (2012) [arXiv:1204.0626 [hep-ex]].
- [9] K. Abe *et al.* [T2K Collaboration], Phys. Rev. Lett. **112**, 061802 (2014) [arXiv:1311.4750 [hep-ex]].
- [10] D. V. Forero, M. Tortola and J. W. F. Valle, Phys. Rev. D **90**, no. 9, 093006 (2014) [arXiv:1405.7540 [hep-ph]].
- [11] F. Capozzi, G. L. Fogli, E. Lisi, A. Marrone, D. Montanino and A. Palazzo, Phys. Rev. D **89**, no. 9, 093018 (2014) [arXiv:1312.2878 [hep-ph]].
- [12] M. C. Gonzalez-Garcia, M. Maltoni and T. Schwetz, JHEP **1411**, 052 (2014) [arXiv:1409.5439 [hep-ph]].
- [13] S. Fukuda *et al.* [Super-Kamiokande Collaboration], Phys. Lett. B **539**, 179 (2002) [hep-ex/0205075]; Y. Ashie *et al.* [Super-Kamiokande Collaboration], Phys. Rev. D **71**, 112005 (2005) [hep-ex/0501064]. P. Adamson *et al.* [MINOS Collaboration], Phys. Rev. Lett. **106**, 181801 (2011) [arXiv:1103.0340 [hep-ex]]. T. Araki *et al.* [KamLAND Collaboration], Phys. Rev. Lett. **94**, 081801 (2005) [hep-ex/0406035].
- [14] P. F. Harrison, D. H. Perkins and W. G. Scott, Phys. Lett. B **458**, 79 (1999) [hep-ph/9904297].
- [15] S. F. King and C. Luhn, Rept. Prog. Phys. **76**, 056201 (2013) [arXiv:1301.1340 [hep-ph]].
- [16] E. Ma and G. Rajasekaran, Phys. Rev. D **64** (2001) 113012 [hep-ph/0106291].
- [17] G. Altarelli and F. Feruglio, Nucl. Phys. B **741**, 215 (2006) [hep-ph/0512103].
- [18] J. Barry and W. Rodejohann, Phys. Rev. D **81**, 093002 (2010) Erratum: [Phys. Rev. D **81**, 119901 (2010)] [arXiv:1003.2385 [hep-ph]].



- [19] B. Karmakar and A. Sil, Phys. Rev. D **91**, 013004 (2015) [arXiv:1407.5826 [hep-ph]] and references therein.
- [20] B. Karmakar and A. Sil, Phys. Rev. D **93**, no. 1, 013006 (2016) [arXiv:1509.07090 [hep-ph]] and references therein.
- [21] Y. Shimizu, M. Tanimoto and A. Watanabe, Prog. Theor. Phys. **126**, 81 (2011) [arXiv:1105.2929 [hep-ph]].
- [22] S. F. King and C. Luhn, JHEP **1109**, 042 (2011) [arXiv:1107.5332 [hep-ph]].
- [23] M. Hirsch, S. Morisi and J. W. F. Valle, Phys. Lett. B **679**, 454 (2009) [arXiv:0905.3056 [hep-ph]].
- [24] G. Altarelli and F. Feruglio, Rev. Mod. Phys. **82**, 2701 (2010) [arXiv:1002.0211 [hep-ph]].
- [25] L. Dorame, S. Morisi, E. Peinado, J. W. F. Valle and A. D. Rojas, Phys. Rev. D **86**, 056001 (2012) [arXiv:1203.0155 [hep-ph]].
- [26] M. Abbas, S. Khalil, A. Rashed and A. Sil, Phys. Rev. D **93**, no. 1, 013018 (2016) [arXiv:1508.03727 [hep-ph]]; S. Fraser, E. Ma and O. Popov, Phys. Lett. B **737**, 280 (2014) [arXiv:1408.4785 [hep-ph]]; E. Ma and R. Srivastava, Mod. Phys. Lett. A **30**, no. 26, 1530020 (2015) [arXiv:1504.00111 [hep-ph]]; A. Mukherjee and M. K. Das, Nucl. Phys. B **913**, 643 (2016) [arXiv:1512.02384 [hep-ph]].
- [27] K. Asakura *et al.* [KamLAND-Zen Collaboration], AIP Conf. Proc. **1666**, 170003 (2015) [arXiv:1409.0077 [physics.ins-det]].
- [28] J. B. Albert *et al.* [EXO-200 Collaboration], Nature **510**, 229 (2014) [arXiv:1402.6956 [nucl-ex]].
- [29] M. Lindner, M. A. Schmidt and A. Y. Smirnov, JHEP **0507**, 048 (2005) [hep-ph/0505067].
- [30] K. A. Olive *et al.* [Particle Data Group Collaboration], Chin. Phys. C **38**, 090001 (2014).
- [31] X. G. He and A. Zee, Phys. Lett. B **645**, 427 (2007) [hep-ph/0607163].
- [32] C. H. Albright and W. Rodejohann, Eur. Phys. J. C **62**, 599 (2009) [arXiv:0812.0436 [hep-ph]].
- [33] G. Altarelli, F. Feruglio, L. Merlo and E. Stamou, JHEP **1208**, 021 (2012) [arXiv:1205.4670 [hep-ph]].

- [34] P. A. R. Ade *et al.* [Planck Collaboration], arXiv:1303.5076 [astro-ph.CO].
- [35] S. Antusch, C. Biggio, E. Fernandez-Martinez, M. B. Gavela and J. Lopez-Pavon, JHEP **0610**, 084 (2006) [hep-ph/0607020].
- [36] M. C. Gonzalez-Garcia and J. W. F. Valle, Phys. Lett. B **216**, 360 (1989).
- [37] K. Kanaya, Prog. Theor. Phys. **64**, 2278 (1980).
- [38] G. Altarelli and D. Meloni, Nucl. Phys. B **809**, 158 (2009) [arXiv:0809.1041 [hep-ph]].
- [39] S. Antusch, J. P. Baumann and E. Fernandez-Martinez, Nucl. Phys. B **810**, 369 (2009) [arXiv:0807.1003 [hep-ph]].
- [40] P. S. B. Dev and R. N. Mohapatra, Phys. Rev. D **81**, 013001 (2010) [arXiv:0910.3924 [hep-ph]].
- [41] A. G. Dias, C. A. de S.Pires, P. S. Rodrigues da Silva and A. Sampieri, Phys. Rev. D **86**, 035007 (2012) [arXiv:1206.2590].
- [42] A. Ilakovac and A. Pilaftsis, Nucl. Phys. B **437**, 491 (1995) [hep-ph/9403398].
- [43] R. Alonso, M. Dhen, M. B. Gavela and T. Hambye, JHEP **1301**, 118 (2013) [arXiv:1209.2679 [hep-ph]].
- [44] T. Hahn, physics/0607103.
- [45] R. Lal Awasthi and M. K. Parida, Phys. Rev. D **86**, 093004 (2012) [arXiv:1112.1826 [hep-ph]].
- [46] M. K. Parida, R. L. Awasthi and P. K. Sahu, JHEP **1501**, 045 (2015) [arXiv:1401.1412 [hep-ph]].
- [47] M. K. Parida and B. P. Nayak, arXiv:1607.07236 [hep-ph].
- [48] S. M. Bilenky, S. T. Petcov and B. Pontecorvo, Phys. Lett. **67B**, 309 (1977).
- [49] B. He, T. P. Cheng and L. F. Li, Phys. Lett. B **553**, 277 (2003) [hep-ph/0209175].
- [50] D. V. Forero, S. Morisi, M. Tortola and J. W. F. Valle, JHEP **1109**, 142 (2011) [arXiv:1107.6009 [hep-ph]].
- [51] L. Delle Rose, C. Marzo and A. Urbano, JHEP **1512**, 050 (2015) [arXiv:1506.03360 [hep-ph]].

- [52] C. Bonilla, J. W. F. Valle and J. C. Romo, Phys. Rev. D **91**, no. 11, 113015 (2015) [arXiv:1502.01649 [hep-ph]].
- [53] C. Bonilla, R. M. Fonseca and J. W. F. Valle, Phys. Lett. B **756**, 345 (2016) [arXiv:1506.04031 [hep-ph]].
- [54] M. Mitra, G. Senjanovic and F. Vissani, Nucl. Phys. B **856**, 26 (2012) [arXiv:1108.0004 [hep-ph]].
- [55] J. Chakraborty, H. Z. Devi, S. Goswami and S. Patra, JHEP **1208**, 008 (2012) [arXiv:1204.2527 [hep-ph]].
- [56] A. S. Joshipura and J. W. F. Valle, Nucl. Phys. B **397**, 105 (1993). A. S. Joshipura and S. D. Rindani, Phys. Rev. Lett. **69**, 3269 (1992). J. C. Romao, F. de Campos and J. W. F. Valle, Phys. Lett. B **292**, 329 (1992) [hep-ph/9207269].
- [57] V. Tello, M. Nemevsek, F. Nesti, G. Senjanovic and F. Vissani, Phys. Rev. Lett. **106**, 151801 (2011) [arXiv:1011.3522 [hep-ph]].
- [58] S. Khan, S. Goswami and S. Roy, Phys. Rev. D **89**, no. 7, 073021 (2014) [arXiv:1212.3694 [hep-ph]].
- [59] P. S. Bhupal Dev, R. Franceschini and R. N. Mohapatra, Phys. Rev. D **86**, 093010 (2012) [arXiv:1207.2756 [hep-ph]].
- [60] A. Das, P. S. Bhupal Dev and N. Okada, Phys. Lett. B **735**, 364 (2014) [arXiv:1405.0177 [hep-ph]].